Envisioning an Optimal Network of Space-Based Lasers for Orbital Debris Remediation

David O. Williams Rogers[a], Matthew C. Fox[a], Paul R. Stysley[b], Hang Woon Lee[a,*]

[a]*Department of Mechanical, Materials and Aerospace Engineering, West Virginia University, 1306 Evansdale Drive, Morgantown, 26506, WV, USA*
[b]*NASA Goddard Space Flight Center, 8800 Greenbelt Rd, Greenbelt, 20771, MD, USA*

Abstract

The rapid increase in resident space objects, including satellites and orbital debris, poses a significant threat to the safety and sustainability of space missions. This paper explores orbital debris remediation using a network of collaborative space-based lasers, leveraging laser ablation for momentum transfer on debris. A novel delta-v vector analysis framework quantifies the effects of multiple simultaneous laser-to-debris (L2D) engagements by using vector composition of the imparted delta-v vectors. The paper introduces the Concurrent Location-Scheduling Problem (CLSP), which optimizes the placement of laser platforms and the scheduling of L2D engagements to maximize debris remediation capacity. Due to the computational complexity of the CLSP, it is decomposed into two sequential subproblems: (1) optimal laser platform locations are determined using the Maximal Covering Location Problem, and (2) a novel integer linear programming-based approach schedules L2D engagements within the network configuration to maximize remediation capacity. Computational experiments are conducted to evaluate the proposed framework's effectiveness under various mission scenarios, demonstrating key network functions such as collaborative nudging, deorbiting, and just-in-time collision avoidance. A sensitivity analysis further examines how varying the number and distribution of laser platforms affects debris remediation capacity, providing insights into optimizing the performance of space-based laser networks.

Keywords: Space-based lasers, orbital debris remediation, network optimization, facility location problems, integer linear programming

1. Introduction

The number of resident space objects is rapidly increasing, largely due to the emergence of small satellites, owing to standardized manufacturing processes,

*Corresponding Author.

advancements in technology, and lower costs for sharing space on launch vehicles. This increase in the number of satellites is correlated with the significant growth in orbital debris, posing a serious risk to both manned and unmanned missions as well as active satellites that form critical infrastructure, yielding an escalation in conjunction alerts (*e.g.,* satellites approaching within 3 km [1]) and an increased probability of in-space collisions, which can create debris clouds of varying sizes.

Large orbital debris, objects with characteristic lengths greater than 10 cm, is identified as the primary source of new debris [2] and consists mostly of defunct satellites, payloads, and rocket stages. Its presence in orbit increases the cost of operations, requiring active satellites to perform collision avoidance maneuvers, thereby demanding additional fuel consumption, the loss of mission objectives due to maneuvering, and increased labor costs for planning these maneuvers. Additionally, large debris restricts access to space for new satellites or payloads, affecting activities that heavily rely on space infrastructure, such as telecommunications, financial exchanges, and climate monitoring [3].

Conversely, small debris comprises objects with characteristic lengths between 1 and 10 cm. The challenges of tracking small debris pieces, coupled with their significant population close to 500,000 objects [4], present a continuous threat of collisions in space. Even with their relatively small mass, these fragments have the potential to inflict hypervelocity impacts, penetrating spacecraft shielding and risking the success of the mission. The origins of small debris include loose parts from operational or defunct satellites, payloads, or rocket stages, such as sodium-potassium droplets, solid rocket motor slag and dust, multi-layer insulation, ejecta, and paint flakes [5]. Notably, a significant part of the population has been generated by anti-satellite tests [6], accidental explosions of satellites and rocket bodies [7], and debris-to-debris collisions [8].

Considering the substantial size of the debris population and the looming threat of triggering the Kessler syndrome [9], strategies limited to the prevention of new debris formation, such as implementing regular conjunction assessments for active spacecraft [10] and enforcing restrictions on mission operations and end-of-life procedures [4] are insufficient for addressing the debris problem comprehensively. In response to this, a range of promising and innovative debris remediation technologies has been proposed to reduce the debris population.

The literature on debris remediation introduces contact-based methods as strategies for eliminating orbital debris. Chaser spacecraft equipped with tethered nets are considered an effective debris remediation mechanism [11] for addressing irregularly shaped debris. Space balls and space winches are mechanisms designed to tackle the problem of debris with high angular momentum. These methods are capable of exerting a retarding torque on debris, aiding in its stabilization. However, they require an accurate activation at the time of the engagement [12]. For relatively stable (*i.e.,* detumbled) objects, debris remediation mechanisms such as grappling can be implemented for targeted and controlled removal. For instance, spacecraft equipped with robotic arms can accomplish this task [13], by leveraging a rendezvous maneuver to capture the target and subsequently relocating it into a disposal orbit or into an orbit where atmospheric effects induce reentry. However, this technique is highly dependent

on the physical properties of the debris, such as its shape and surface texture. It also necessitates precise attitude adjustment to counteract the forces exerted by the robotic arm's movements [14]. Hooks and harpoons are penetrating mechanisms used for debris remediation; however, they require proximity operations, endangering the success of the mission, and during penetration, they can trigger an explosion [12] generating more debris pieces.

Unlike the contact-based debris remediation mechanisms described above, which are targeted at large debris, remediating small debris requires specific methods compatible with their size. Novel tethered plate systems, capable of remediating debris pieces without damaging the plate's structure, have been proposed [15]. Furthermore, perimeter-ring-truss systems can handle small debris while ensuring scalability and practicality in the design phase [16]. However, the cost of remediation per debris piece is analyzed to be the highest in comparison with other methods [3].

Ground-based lasers have emerged as a promising, cost-effective debris remediation solution to address the growing orbital debris population while circumventing the challenges and limitations of contact-based debris remediation methods. The change in velocity, Δv, required to reduce the target's orbit altitude can be imparted by a ground-based laser leveraging photon pressure or laser ablation mechanisms. Photon pressure-based lasers exert a small force on the target object sufficient to induce small orbit changes. Mason et al. [17] present the use of two photon pressure ground-based laser systems, to engage debris multiple times and change its orbit due to the applied perturbation, thereby ultimately avoiding collisions with operational satellites. However, given the laser's wavelength, debris temperature, and material properties, there is a threat of generating specular reflections on the debris surface (*i.e.,* Iridium flares), which scale linearly with the laser power (excluding thermal properties) [18]. In light of the small forces that photon pressure imparts on the target, its application is constrained to collision avoidance only [18]. Alternatively, laser ablation mechanisms rely on the laser's high energy to rapidly melt the target's surface and generate a material jet that produces a reactive momentum, typically higher than the one produced by photon pressure-based lasers [18]. On the one hand, continuous wave heating produces irregular melt ejection, which can generate more debris. In the case of a tumbling target, the average momentum transfer can be nullified due to the slow heating and decay characteristic of the imparted thrust [19]. On the other hand, pulsed lasers appear as a mechanism suitable for collision avoidance and deorbiting debris, given that the per pulse energy delivered from the ground-based station is enough to change debris orbit [20].

Despite their promise as debris remediation solutions, ground-based laser debris remediation systems face significant technical challenges. These systems are subject to numerous atmospheric constraints, including aerosol attenuation, cloud cover, scintillation effects, and turbulence, all of which affect beam quality [17]. Moreover, ground-based lasers have limitations in range and angles and thus require strategic positioning of their ground stations to maximize efficiency while considering various civil and operational constraints (*i.e.,* ideally situated away from airports and air routes) [20]. Ultimately, given their ground-based na-

ture, laser engagement opportunities depend on debris passing over the systems' operational range, constraining ground-based lasers to preventive just-in-time collision avoidance without the ability to tackle immediate collision threats [21].

Against this backdrop, the idea of space-based lasers has garnered increased attention over the past decade, owing to their capacity to address debris of varying sizes (both large and small) and their potential to overcome the inherent challenges associated with ground-based lasers [22, 21, 23, 24, 25, 26, 27]. Space-based lasers possess several advantages compared to their ground-based counterparts, including more efficient energy delivery and beam quality [21], increased access to debris (contact duration and opportunities) [24], and reduced risk of collateral damage due to more precise control enabled by shorter ranges [28]. According to the NASA Cost and Benefit Analysis of Orbital Debris Remediation report [3], ground-based and space-based laser systems are debris remediation methods that can handle both trackable and non-trackable debris pieces with the best cost-to-benefit remediation ratio. Moreover, when not used for remediation purposes, the operator can rely on them to track and characterize debris objects [3].

The existing literature on space-based lasers successfully validates the concept of debris remediation for different sizes; however, several research gaps need to be addressed to make such systems attractive. First, constraining the number of platforms to one or two cannot scale up efficiently to a more extensive debris population, which is rapidly expanding every year and is highly heterogeneous in materials, size, density, and orbital parameters. Further, the effectiveness of laser ablation is heavily influenced by the irradiation distance, angle, and revisit time, posing a challenge for a single or two laser platforms arbitrarily located in space. Second, while nudging debris or placing it on a descent trajectory can alleviate immediate threats to specific valuable assets, it may inadvertently create hazardous conjunction events for other objects in space.

In response to these challenges, we envision a network of interconnected, collaboratively working space-based lasers, optimally designed to maximize the debris remediation capacity, that is, the ability to nudge and deorbit debris and perform just-in-time collision avoidance. Aiming to materialize this concept, we address the following research questions in this paper:

1. *"Where do we optimally locate the space-based laser platforms with respect to each other and the debris field?"*

2. *"How do we optimally schedule laser-to-debris engagements such that the debris remediation capacity is maximized?"*

We advance the state of the art in several ways. First, we propose a vector analysis of the Δv's imparted by multiple laser platforms, which we name Δv *Vector Analysis* (DVA). Employing multiple lasers increases the degrees of freedom in the debris control mechanism for remediation missions. This allows for finer control over the target debris resultant Δv magnitude and direction, offering a wider range of potential paths for its subsequent descent or collision avoidance trajectory. Second, we propose the *Concurrent Location-Scheduling*

Optimization Problem (CLSP), an integer linear programming (ILP) formulation that seeks to simultaneously determine the optimal location for a set of laser platforms while scheduling the L2D engagements leveraging the concept of DVA. As a consequence of the explosion in the solution space for the CLSP, we decompose the original problem into two. The location problem is solved by leveraging the formulation of the *Maximal Covering Location Problem* (MCLP) [29, 30, 31], typically found in the literature on facility location problems, to design an optimal network topology that maximizes laser engagement rewards with the debris field. In its original domain, MCLP aims to find the optimal locations for a set of facilities to maximize coverage over a set of customers. We exploit the similarities between satellite constellation pattern design and facility location problems, as discussed in Ref. [31], interpreting the facilities as laser platforms and the debris as customers. The scheduling problem is addressed by proposing a novel integer linear programming (ILP)-based formulation, referred to as the *laser-to-debris (L2D) engagement scheduling problem* (ESP). This formulation determines which combination of lasers should engage with which debris, considering a reward function that accounts for debris mass, change in periapsis radius, and the risk of potential conjunctions with operational satellites before and after the engagements. Third, each optimization model takes as input parameters the debris field, valuable assets, the risk of potential conjunctions between them, the number of platforms, and their laser specifications, including pulse energy, pulse length, and operational range.

Case studies considering (1) small debris only, (2) large debris only, and (3) a mixed debris field along with 10 valuable assets are presented to illustrate the extension of the framework. For all three case studies, the framework presented in this paper outperforms Walker-Delta [32]-based networks with the same number of platforms in terms of the debris remediation capacity. Additionally, we present a sensitivity analysis to characterize the impact of varying the number of laser platforms on debris remediation capacity. For the case studies presented in this paper, we adopt the L'Adroit laser platform [24] given its ability to tackle both large and small debris objects. It is noteworthy to mention that different laser systems can be used to design and operate the network and that the design and validation of a specific laser system are outside the scope of this paper.

The rest of the paper is structured as follows: Sec. 2 describes the technical details of the laser ablation process and DVA. Section 3 presents the parameter generation and the mathematical optimization formulation. Section 4 illustrates the case studies with debris fields of diverse sizes. Section 6 outlines the limitations of this paper, and Sec. 7 presents the conclusions of this paper.

2. Laser-to-Debris Engagement Modeling

In this paper, space-based laser platforms engage debris by irradiating a laser beam, inducing a laser ablation process that alters the debris orbit. The governing dynamics of the laser ablation process are described in Sec. 2.1 and the DVA mechanism is presented in Sec. 2.2.

The L2D framework is built upon several assumptions. First, debris is considered to be a perfect sphere. Second, all L2D engagements are deterministic, meaning that the position and velocity of debris after the engagement are known. Third, each laser platform has complete knowledge of the characteristics of debris (*e.g.,* material, mass, orbit) and whether they endanger the safe operation of valuable in-space assets, for instance, the International Space Station, and in-service telecommunications and Earth-observation satellites. Finally, we assume that the space-based laser network operates as a centralized system with global knowledge. In this system, each platform is aware of the magnitude and direction that all other platforms in the network can impart over debris, as well as their orbital states during the mission.

We define the mission time horizon as a set of uniformly discretized time steps $\mathcal{T} = \{t_0, \ldots, t_{T-1}\}$, with index t and cardinality T, where t_0 corresponds to the epoch. The laser platform set is defined as $\mathcal{P} = \{p_1, \ldots, p_P\}$ with index p and cardinality P, and the debris set $\mathcal{D} = \{d_1, \ldots, d_D\}$ with index d and cardinality D.

2.1. Laser Ablation Principle

Pulsed laser ablation is the process by which a solid ejects plasma from its surface due to the action of a short, intense laser pulse [33]. At regimes of high irradiance, the vaporized surface material becomes ionized and begins to absorb the incident laser beam leading to vapor breakdown and plasma formation [34]. The ablation rate, defined as the thickness of the ablated material per laser pulse, is inversely proportional to the square root of the beam diameter, and negatively correlated with laser wavelength given the reduced optical absorptivity and high reflectivity of targets at large wavelengths [35]. Given the velocity of the ejected material, and by the principle of momentum conservation, the ejected mass of the plasma generates a net impulse on the object [36].

Pulsed laser ablation can be leveraged to impart an impulse to debris, causing a change in velocity that alters the size and/or shape of its resulting orbit. The magnitude of this perturbation is determined by laser parameters such as wavelength, output power, pulse energy, beam quality, and the length and frequency of pulses [37, 38], as well as by the properties of the target debris, including its mass, density, and surface material composition [28, 39, 40]. Moreover, the geometric relationship between the laser and debris determines the direction and magnitude of the velocity perturbation applied to the debris, influencing the resulting orbit.

The momentum coupling factor c_m relates the imparted impulse on debris with the used laser's pulse optical energy [41], and is defined as [40]:

$$m\Delta v = c_\mathrm{m} E$$

where E is the laser energy delivered to the debris by a single pulse and m is the debris mass. Further, the on-debris delivered laser fluence φ is defined as [24]:

$$\varphi = \frac{4ED_\mathrm{eff}^2 T_\mathrm{tot}}{\pi B^4 \zeta^2 \lambda^2 u^2}$$

with D_{eff}^2 being the effective illuminated beam diameter, T_{tot} the total system loss factor, B the beam quality factor, ζ a constant that regulates diffraction, λ the wavelength, and u the range between the platform and debris. Consequently, the per-pulse L2D Δv delivered on debris with surface mass ρ is given as:

$$\Delta v = \eta \frac{c_{\text{m}} \varphi}{\rho} \tag{1}$$

where η is the impulse transfer efficiency, which takes into account shape effects, tumbling, improper thrust direction on debris, and other factors [24].

2.2. Δv Vector Analysis

In this section, we present the DVA, a novel framework to quantify the effects of multiple simultaneous L2D engagements on target debris by leveraging a vector composition of the imparted $\Delta \boldsymbol{v}$ vectors.

We let $\boldsymbol{r}_{td}^-$ and $\boldsymbol{v}_{td}^-$ indicate the position and velocity vectors, respectively, of debris d at time step t immediately before an L2D engagement. Similarly, $\boldsymbol{r}_{td}^+$ and $\boldsymbol{v}_{td}^+$ are the position and velocity vectors, respectively, of debris d at time step t immediately after an L2D engagement.

We assume that at time step t an L2D engagement induces an instantaneous change in the velocity of target debris but its position remains unchanged. Hence, we have:

$$\begin{aligned} \boldsymbol{v}_{td}^+ &= \boldsymbol{v}_{td}^- + \Delta \boldsymbol{v}_{tpd} \\ \boldsymbol{r}_{td}^- &= \boldsymbol{r}_{td}^+ = \boldsymbol{r}_{td} \end{aligned}$$

where $\Delta \boldsymbol{v}_{tpd}$ represents the change in velocity experienced by debris d due to an L2D engagement from laser platform p.

At time step t, given position vectors $\boldsymbol{r}_{td}$ and $\boldsymbol{r}_{tp}$ of debris d and platform p, respectively, the relative position vector that points from platform p to debris d is given as $\boldsymbol{u}_{tpd} = \boldsymbol{r}_{td} - \boldsymbol{r}_{tp}$; its unit vector is given as $\hat{\boldsymbol{u}}_{tpd} = \boldsymbol{u}_{tpd}/u_{tpd}$, with $u_{tpd} = \|\boldsymbol{u}_{tpd}\|_2$. The total change in velocity imparted from laser platform p to debris d at time step t is calculated by generalizing Eq. (1) for every time step t, laser platform p, and debris d. Equation (3) presents the vector $\Delta \boldsymbol{v}_{tpd}$ from laser platform p to debris d at time step t given unit vector $\hat{\boldsymbol{u}}_{tpd}$.

$$\Delta \boldsymbol{v}_{tpd} = N_d \frac{\eta_{pd} \varphi_{pd} c_{\text{m},pd}}{\rho_d} \hat{\boldsymbol{u}}_{tpd} \tag{3}$$

where N_d is the number of laser pulses per time step t on debris d, computed from the time step size and the laser pulse repetition frequency (PRF), which denotes the number of laser pulses per second.

The DVA framework captures multiple, simultaneous L2D engagements and represents them as a total effective single L2D engagement. The total $\Delta \boldsymbol{v}_{td}$ over debris d at time step t due to multiple L2D engagements can be represented as follows:

$$\Delta \boldsymbol{v}_{td} = \sum_{p \in \mathcal{P}_{td}} \Delta \boldsymbol{v}_{tpd}$$

where $\mathcal{P}_{td}$ represents the set of laser platforms that engage debris d at time step t. To determine how $\Delta \boldsymbol{v}_{td}$ affects debris trajectory, the new debris orbital parameters (*i.e.,* semi-major axis, eccentricity) can be analytically computed using $\boldsymbol{r}_{td}$ and $\boldsymbol{v}_{td}^{+} = \boldsymbol{v}_{td}^{-} + \Delta \boldsymbol{v}_{td}$ and compared with those before the L2D engagement.

The significance of DVA lies in its ability to enable a higher degree of control over debris dynamics by controlling the imparted $\Delta \boldsymbol{v}$ in both magnitude and direction, thus leading to a new debris orbit. Figure 1 illustrates an example involving two laser platforms acting on the same debris at a given time step. In this specific scenario, there are three different perturbed orbits available for the debris: (1) one acted solely by platform p_1, (2) another acted solely by platform p_2, and (3) one acted collaboratively by both platforms simultaneously, resulting from a combined $\Delta \boldsymbol{v}_{t_1 d} = \Delta \boldsymbol{v}_{t_1 p_1 d} + \Delta \boldsymbol{v}_{t_1 p_2 d}$. The availability of multiple L2D engagement opportunities is advantageous, providing the space-based laser network with greater flexibility to achieve more effective debris remediation.

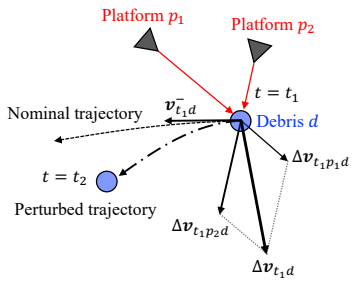

Figure 1: DVA illustrative example with two laser platforms p_1 and p_2 and debris object d.

3. Space-based Lasers Network Design and Operations Optimization

The debris remediation capacity of space-based networks is correlated with the location of laser platforms. Given the distribution of the debris field and its concentration over specific altitude bins, the network's target access rate depends on the orbits taken by the platforms. Further, the laser ablation mechanism depends on the relative geometry between the platforms and debris. Hence, an optimal network topology can increase the effectiveness of laser ablation, leading to a higher debris remediation capacity.

During the debris remediation mission, each platform can present multiple L2D engagement opportunities. The dynamic scheduling of resources enables the network to select the platforms that present the most favorable relative geometry with respect to debris, such that the debris remediation capacity is maximized due to the L2D ablation mechanism.

The remainder of Sec. 3 is organized as follows. In Sec. 3.1, we exhibit the generation of parameters involved in the optimization, and in Sec. 3.2 the debris remediation capacity reward is introduced. Section 3.3 materializes the proposed location-scheduling optimization problem, and Secs. 3.4 and 3.5 present the decoupled location and scheduling optimization problems, respectively.

3.1. Network Optimization Parameters

As a consequence of an L2D engagement, debris can relocate to a new orbit. We define $\mathcal{J}_{td}$ as the set of orbital slots for debris d at time step t. Each orbital slot $j \in \mathcal{J}_{td}$ is associated with the position and velocity vectors defined at time step t to fully define the state of debris orbit. Laser platform orbital slots are defined in set $\mathcal{S}$, indexed by s and with cardinality S. Each laser platform is assumed to take an orbital slot in $\mathcal{S}$ and maintain it during the entire mission. Moreover, we define a set of valuable assets $\mathcal{K}$ with cardinality K.

The feasibility of the L2D engagements is encoded with Boolean parameter W_{tsd}, given as:

$$W_{tsd} = \begin{cases} 1, & \text{if a platform located at orbital slot } s \text{ can engage} \\ & \text{debris } d \text{ at time step } t \\ 0, & \text{otherwise} \end{cases}$$

To determine if an L2D engagement is feasible, two conditions must be satisfied. First, debris d has to be in the line-of-sight of a laser platform located at orbital slot s at time step t. Given the relative position vector $\boldsymbol{u}_{tsd}$ and the range $u_{tsd} = ||\boldsymbol{u}_{tsd}||_2$, Eq. (4) computes the line-of-sight indicator.

$$q_{tsd} = \left((r_{ts})^2 - (R_{\oplus} + \epsilon)^2\right)^{1/2} + \left((r_{td})^2 - (R_{\oplus} + \epsilon)^2\right)^{1/2} - u_{tsd} \tag{4}$$

where $R_{\oplus}$ is the radius of the Earth and ϵ is a bias parameter. If $q_{tsd} > 0$ debris is in the line-of-sight of a platform and $q_{tsd} \leq 0$ otherwise. Second, as defined in Ref. [22], an L2D engagement can happen if u_{tsd} lies within the maximum and minimum operational ranges defined as $u^d_{\max}$ and $u^d_{\min}$, respectively. The upper bound is determined by the given laser specifications, and the lower bound is set by considering the safety and operational aspects of the system. Leveraging parameter W_{tsd}, it is possible to generate for each time step t the set of laser platform orbital slots $\mathcal{S}_{tdj}$, with index s and cardinality S_{tdj}, that engage debris $d \in \mathcal{D}$ and generate debris orbital slot $j \in \mathcal{J}_{t+1,d}$.

3.2. Laser-to-Debris Engagement Reward

We introduce debris remediation capacity reward R_{tdij} to quantify the value of relocating debris d from its current orbital slot $i \in \mathcal{J}_{td}$ to a new orbital slot $j \in \mathcal{J}_{t+1,d}$ at time step t, as a consequence of an L2D engagement while considering potential conjunctions with the set of valuable assets $\mathcal{K}$. It is defined as:

$$R_{tdij} = C^0_{td} + C_{tdij} + \alpha \Delta h_{tdij} + \beta M_{td} \tag{5}$$

First, C^0_{td} is an incentive term that accounts for the conjunction analysis between debris d and the set of valuable assets $\mathcal{K}$ during the entire mission scenario assuming no L2D engagements, by checking if debris orbit lies inside the deterministic conjunction ellipsoid of any valuable asset in $\mathcal{K}$. We define C^0_{td} as:

$$C^0_{td} = \begin{cases} G_0, & \text{if } t \in [t_{\min}, t_{\max}] \\ 0, & \text{otherwise} \end{cases}$$

If a conjunction, or multiple ones, is feasible between debris d and any valuable asset $\mathcal{K}$, $C^0_{td} = G_0$ for all $t \in [t_{\min}, t_{\max}]$ where G_0 is a large positive constant that incentivizes the network to engage debris during the time window $[t_{\min}, t_{\max}]$. The length of the interval and its starting point are parameters to be defined by a user considering the characteristics of the space-based laser, its capability for changing debris orbits, and the desired miss distance. Given t_c, the time step at which the first conjunction occurs (if debris d is to have multiple conjunctions with the same valuable asset or with several ones), $t_{\max}$ should be defined such that $t_{\max} \leq t_c$. Figure 2a illustrates a scenario where reward C^0_{td} is not activated since there is no feasible conjunction. Figure 2b outlines the case where a conjunction is imminent and the reward is activated.

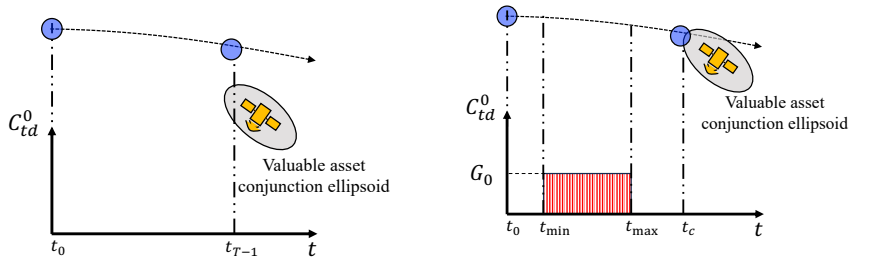

(a) Mission scenario with $C^0_{td} = 0$.

(b) Mission scenario with $C^0_{td} = G_0$ for all $t \in [t_{\min}, t_{\max}]$.

Figure 2: Generation of C^0_{td} reward for two different scenarios.

Second, C_{tdij} is a look-a-head penalty term that accounts for whether relocating debris d from orbital slot i to orbital slot j due to an L2D engagement at time step t triggers at least one conjunction with any valuable asset in $\mathcal{K}$. Once all debris' candidate orbital slots are generated for step $t+1$, each orbital slot is propagated from $t+1$ to $t+1+\tau$, where τ represents the number of look-a-head time steps. Further, we compare for every $t \in [t+1, t+1+\tau]$ if the range between debris d at slot j with any valuable asset is less than the range threshold. If a specific L2D engagement with debris generates a conjunction with any valuable asset defined in $\mathcal{K}$, we set $C_{tdij} = -G$ to ensure that the network is discouraged from relocating debris d to orbital slot j, as illustrated in Fig. 3a. Conversely, Fig. 3b highlights two simultaneous L2D engagements where the resultant debris orbital slot does not invade the valuable asset's conjunction ellipsoid; hence C_{tdij} is not activated.

Third, Δh_{tdij} is a look-a-head incentive term that compares the periapsis radius of debris d orbital slot j after an L2D engagement at time step t with the periapsis radius threshold h^*, at which we consider that debris is governed by atmospheric drag and subject to induced natural orbital decay. Once this decay is initiated, the debris is considered deorbited within the framework. Given $h_{t+1,dj}$, the periapsis radius of the new orbital slot j for debris d after an L2D

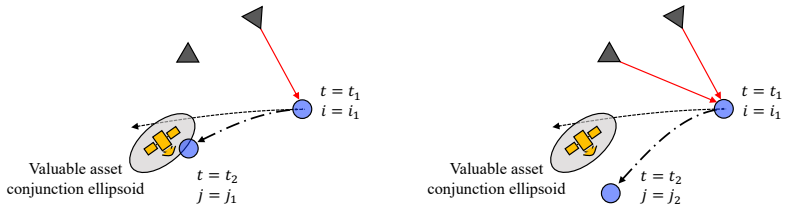

(a) Mission scenario with activated penalty $C_{tdij} = -G$.

(b) Mission scenario with inactive penalty $C_{tdij} = 0$.

Figure 3: Generation of C_{tdij} penalty for two different engagement scenarios.

engagement, the reward term is defined as:

$$\Delta h_{tdij} = \gamma_{tdij} \left(\frac{h^*}{h_{t+1,dj}} \right)^3$$

where γ_{tdij} is a variable that compares the periapsis radius of debris d between initial orbital slot i at time step t and after the L2D engagement at final orbital slot j at time step $t+1$, defined as:

$$\gamma_{tdij} = \begin{cases} -G_h, & \text{if } h_{t+1,dj} \geq h_{tdi} \\ 1, & \text{otherwise} \end{cases}$$

If an L2D engagement increases the periapsis radius, then a large negative constant G_h is assigned to γ_{tdij} to discourage the engagement. Furthermore, given that Δh_{tdij} is a parameter that captures the ratio between the periapsis radius threshold and debris orbit periapsis radius after the engagement, a value of $\Delta h_{tdij} \geq 1$ implies that the object is deorbited; hence, we constrain it to be at most one to avoid obtaining large rewards due to the nature of the terms' formulation. Additionally, we scale it by α in Eq. (5) giving more flexibility to the user.

Lastly, M_{td} accounts for debris d mass, which is activated if debris is engaged at time step t, and whose objective in the reward formulation is two-fold. First, debris of large mass is identified as the main source of new debris in case of a collision, and therefore in alignment with Refs. [2] and [42], which assign a debris remediation capacity reward to debris proportional to its mass, we aim to assign a bigger reward for engaging debris of larger mass. Second, given Eq. (3), it is clear that for the same laser and c_{m} parameters, debris of larger mass will have a smaller Δv than those of smaller mass, making it harder to achieve significant changes in its trajectory, resulting in a smaller Δh_{tdij}. To address the two key points stated above, we introduce the mass reward term, defined as:

$$M_{td} = \begin{cases} m_d / m_{\max}, & \text{if debris } d \text{ is engaged at step } t \\ 0, & \text{otherwise} \end{cases}$$

where $m_{\max}$ is the maximum debris mass in $\mathcal{D}$. We normalize the mass of debris d dividing it by the maximum debris mass to be consistent in terms of magnitude with Δh_{tdij}. Further, we introduce β in Eq. (5) to scale it with respect to other parameters.

3.3. The Concurrent Location-Scheduling Optimization Problem

The optimal mission design and operation of a network of space-based lasers is tackled by proposing the CLSP. This problem seeks to determine the optimal location for a set of platforms while considering an optimal L2D engagement scheduling to maximize the debris remediation capacity.

3.3.1. Decision Variables

We model the placement of laser platforms using the following *platform location decision variables*:

$$z_s = \begin{cases} 1, & \text{if a laser platform is located at orbital slot } s \\ 0, & \text{otherwise} \end{cases}$$

Similarly, we leverage the following *L2D engagement decision variables*:

$$y_{tsd} = \begin{cases} 1, & \text{if a laser platform located at orbital slot } s \text{ engages} \\ & \text{debris } d \text{ at time step } t \\ 0, & \text{otherwise} \end{cases}$$

At each time step t, debris d is enforced to take a new orbital slot $j \in \mathcal{J}_{t+1,d}$. The set of debris orbital slots can be subdivided into two subsets. First, $\tilde{\mathcal{J}}_{t+1,d} \subseteq \mathcal{J}_{t+1,d}$ with index j and cardinality $\tilde{J}_{t+1,d}$ contains the orbital slots that encode no changes in the current orbit for debris d since it is not engaged, and consequently they have no associated reward. Second, the set of new orbits, each one with its corresponding reward R_{tdij}, is encoded as $\mathcal{J}_{t+1,d} \setminus \tilde{\mathcal{J}}_{t+1,d}$ with index j. In CLSP, *debris relocation decision variables* are given as:

$$x_{tdij} = \begin{cases} 1, & \text{if debris } d \text{ relocates from orbital slot } i \text{ to} \\ & \text{orbital slot } j \text{ at time step } t \\ 0, & \text{otherwise} \end{cases}$$

3.3.2. Constraints and Objective Function

We introduce constraints (6a) to enforce that a laser platform located at orbital slot s engages debris d at time step t only if it satisfies the L2D engagement requirements encoded in parameter W_{tsd}. Constraints (6b) enforce that each platform has at most one L2D engagement per time step.

$$W_{tsd} z_s \geq y_{tsd}, \quad \forall t \in \mathcal{T}, \forall s \in \mathcal{S}, \forall d \in \mathcal{D} \tag{6a}$$

$$\sum_{d \in \mathcal{D}} y_{tsd} \leq 1, \qquad \forall t \in \mathcal{T}, \forall s \in \mathcal{S} \tag{6b}$$

We define path contiguity constraints to ensure the correct flow of debris throughout the entire mission horizon. First, we require all debris to occupy a new orbital slot at time step t_1 with constraints (7). Second, constraints (8) ensure that debris d follows a continuous path between steps $t-1$ and $t+1$ with respect to the intermediate reference slot $i \in \mathcal{J}_{td}$ at time step t.

$$\sum_{j \in \mathcal{J}_{t_1 d}} x_{t_0 d i_0 j} = 1, \qquad \forall d \in \mathcal{D} \tag{7}$$

$$\sum_{j \in \mathcal{J}_{t+1,d}} x_{tdij} - \sum_{v \in \mathcal{J}_{t-1,d}} x_{t-1,dvi} = 0, \quad \forall t \in \mathcal{T} \setminus \{t_0, t_{T-1}\}, \forall d \in \mathcal{D}, \forall i \in \mathcal{J}_{td} \tag{8}$$

Constraints (9) are linking constraints that couple debris relocation decision variables x_{tdij} and L2D engagement decision variables y_{tsd}. A relocation to orbital slot $j \in \mathcal{J}_{t+1,d}$ is only possible if debris d is engaged by a set of laser platforms located at orbital slots in $\mathcal{S}_{tdj}$, which enable such a relocation. We relax $\tilde{\mathcal{J}}_{t+1,d}$ given that it has an associated $\mathcal{S}_{tdj} = \emptyset$ and debris is enforced to occupy only one new orbital slot imposed by constraints (7) and (8).

$$\sum_{s \in \mathcal{S}_{tdj}} y_{tsd} \geq S_{tdj} x_{tdij}, \quad \forall t \in \mathcal{T} \setminus \{t_{T-1}\}, \forall d \in \mathcal{D}, \forall i \in \mathcal{J}_{td}, \forall j \in \mathcal{J}_{t+1,d} \setminus \tilde{\mathcal{J}}_{t+1,d} \tag{9}$$

Additionally, constraint (10) enforces the number of platforms in the network to be equal to P.

$$\sum_{s \in \mathcal{S}} z_s = P \tag{10}$$

The domains of all decision variables are given as follows:

$$z_s \in \{0,1\}, \quad \forall s \in \mathcal{S} \tag{11}$$

$$y_{tsd} \in \{0,1\}, \quad \forall t \in \mathcal{T}, \forall s \in \mathcal{S}, \forall d \in \mathcal{D} \tag{12}$$

$$x_{tdij} \in \{0,1\}, \quad \forall t \in \mathcal{T} \setminus \{t_{T-1}\}, \forall d \in \mathcal{D}, \forall i \in \mathcal{J}_{td}, \forall j \in \mathcal{J}_{t+1,d} \tag{13}$$

Lastly, the model's objective is to maximize the remediation capacity of the network, which is given as:

$$\sum_{t \in \mathcal{T} \setminus \{t_{T-1}\}} \sum_{d \in \mathcal{D}} \sum_{i \in \mathcal{J}_{td}} \sum_{j \in \mathcal{J}_{t+1,d}} R_{tdij} x_{tdij} \tag{14}$$

3.3.3. Mathematical Formulation

Piecing everything together, the mathematical formulation for CLSP is given as follows:

max Objective function (14)
s.t. Constraints (6a), (6b), (7), (8), (9), (10), (11), (12) and (13)

We report all sets, parameters, and variables used in the CLSP mathematical formulation in Table 1.

Table 1: Sets, parameters, and variables for the CLSP model.

Type	Symbol	Description
Sets	$\mathcal{T}$	Mission planning horizon (index t; cardinality T)
	$\mathcal{S}$	Set of orbital slots for laser platforms (index s; cardinality S)
	$\mathcal{D}$	Set of debris (index d; cardinality D)
	$\mathcal{J}_{td}$	Set of debris orbital slots at time step t (index j; cardinality J_{td})
	$\mathcal{S}_{tdj}$	Set of laser platform orbital slots that engage debris d at time step t and generate orbital slot j (index s; cardinality S_{tdj})
Parameters	R_{tdij}	Debris remediation capacity reward for relocating debris d from orbital slot i to orbital slot j at time step t
	W_{tsd}	$\begin{cases} 1, & \text{if debris } d \text{ can be engaged by a platform located at orbital slot } s \text{ at time step } t \\ 0, & \text{otherwise} \end{cases}$
	P	Number of platforms in the network
Decision variables	z_s	$\begin{cases} 1, & \text{if a platform is located at orbital slot } s \\ 0, & \text{otherwise} \end{cases}$
	y_{tsd}	$\begin{cases} 1, & \text{if a platform located at orbital slot } s \text{ engages debris } d \text{ at time step } t \\ 0, & \text{otherwise} \end{cases}$
	x_{tdij}	$\begin{cases} 1, & \text{if debris } d \text{ relocates from orbital slot } i \text{ to orbital slot } j \text{ at time step } t \\ 0, & \text{otherwise} \end{cases}$

3.3.4. Illustrative Example

To illustrate CLSP, we present a small-scale instance with $S = 3$, $T = 3$, $D = 3$, and $P = 2$. Figure 4 outlines the tree structure of the problem with platform orbital slots s represented with rhombus, and debris orbital slots i, j with squares. The magenta lines represent feasible decision variables y_{tsd}, the gray lines are debris d feasible relocation variables x_{tdij} at time step t from orbital slot $i \in \mathcal{J}_{td}$ to the set of orbital slots $j \in \tilde{\mathcal{J}}_{t+1,d}$, and the dark lines are debris feasible relocation variables $x_{tdij}$to orbital slots $j \in \mathcal{J}_{t+1,d} \setminus \tilde{\mathcal{J}}_d^{t+1}$. Unfeasible decision variables are given a large negative reward R_{tdij} and are not displayed in the figure.

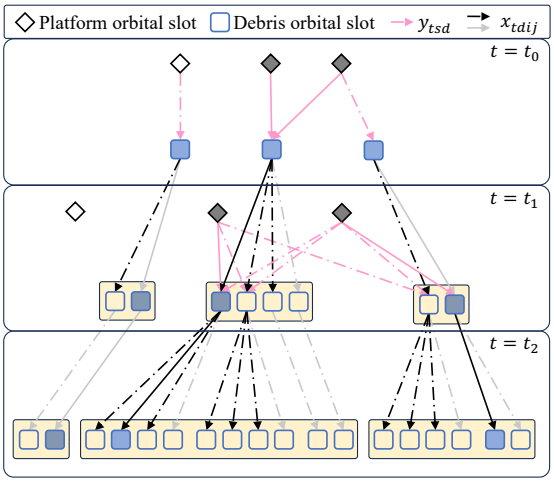

Figure 4: Illustration of the solution space for CLSP.

In Fig. 4 debris is initially located at orbital slot $i \in \mathcal{J}_{t_0 d}$ and has an associated virtual orbital slot $j \in \tilde{\mathcal{J}}_{t_1,d}$, which represents no change in orbit if no L2D engagement occurs, and consequently $R_{t_0 dij} = 0$. The subset of debris orbital slots that represent new orbits depends on the number of feasible L2D engagements, for instance, while the leftmost debris can be engaged only by the leftmost platform orbital slot, debris located in the center orbital slot can be engaged by at most two platforms, hence it has three new orbits, all of them with its corresponding reward $R_{t_0 dij}$. Given that, at time step t_1 the number of total debris orbital slots is eight and that the number of possible L2D engagements is seven, the total number of debris orbital slots at time step t_2 expands to 18.

The problem has 94 integer binary variables and 85 constraints and is solved using the Gurobi optimizer 11, which retrieves an objective value (*i.e.,* debris remediation capacity reward obtained) of 7.50 with a duality gap of 0.00 %. In Fig. 4 the selected platform orbital slots are colored in dark gray, the debris orbital slots in blue, and decision variables $y_{tsd} = 1$ and $x_{tdij} = 1$ are straight lines, conversely, decision variables equal to zero are represented with dashed lines.

Even though the problem is presented for a small number of time steps and orbital slots, the number of decision variables and constraints grows exponentially. Further, Fig. 4 accurately showcases the tree structure of the problem and how it rapidly expands. Scaling this formulation for larger mission horizons with more debris and platform orbital slots makes the problem computationally prohibitive, restricting its application to small-scale problems.

To overcome this challenge, we propose two separate optimization formulations. First, we find the optimal laser network topology design using MCLP, then, we leverage it to optimize the debris remediation capacity using the L2D-

ESP.

3.4. Optimal Laser Network Topology Design

The problem of designing an optimal laser network topology is tackled under the assumption that debris does not relocate; consequently, decision variables x_{tdij} are relaxed, that is, removed, along with constraints (7), (8), (9) and (13). The resulting formulation inherits the location-scheduling structure from CLSP with location decision variables z_s, L2D engagement decision variables y_{tsd} and an orbital slot-independent reward, given as:

$$R_{td} = C^0_{td} + M_{td} \tag{15}$$

The network topology reward R_{td} accounts for feasible conjunctions between debris d and any valuable asset in $\mathcal{K}$ leveraging parameter C^0_{td} and for the mass of the engaged debris d with parameter M_{td}, both introduced in Eq. (5). However, the new reward R_{td} cannot assess whether that L2D potential interaction will effectively lower debris periapsis radius because the Δh_{tdij} term from Eq. (5) is relaxed. To address this problem, we introduce Boolean parameter W'_{tsd}, defined as:

$$W'_{tsd} = \begin{cases} 1, & \text{if } W_{tsd} = 1 \text{ and } h_{t+1,dj} \leq h_{tdi} \\ 0, & \text{otherwise} \end{cases}$$

Given the nature of reward R_{td}, the new formulation can prioritize the selection of platform orbital slots closer to larger debris and neglect orbital slots that can engage small debris objects since the change in debris periapsis radius is not considered in the reward. Further, the resulting topology which is concentrated over larger debris, can considerably reduce the L2D engagement opportunities during the L2D-ESP described in Sec. 3.5. To tackle this problem, we propose to leverage MCLP to design an optimal laser network topology. We refer the reader to Appendix A for an in-depth justification.

3.4.1. Decision Variables

To formulate our problem as an MCLP, we keep platform location decision variables z_s and introduce new decision variables x_{td} defined as:

$$x_{td} = \begin{cases} 1, & \text{if debris } d \text{ is engaged at time step } t \\ 0, & \text{otherwise} \end{cases}$$

These new decision variables are distinct from CLSP L2D engagement decision variables y_{tsd} in a manner that they encode if debris is engaged or not and do not discriminate which platforms perform L2D ablation over debris.

3.4.2. Constraints and Objective Function

In light of the fact that no L2D engagement can occur between a platform located at orbital slot s and debris d if orbital slot s is not taken, linking constraints (16) between decision variables z_s and x_{td} are imposed. Decision

variables x_{td} are activated if at least $S_{td} \in \mathbb{Z}_{\geq 1}$ platforms engage debris d at time step t.

$$\sum_{s \in \mathcal{S}} W'_{tsd} z_s \geq S_{td} x_{td}, \quad \forall t \in \mathcal{T}, \forall d \in \mathcal{D} \tag{16}$$

Here, S_{td} is a parameter inspired from the cardinality of set $\mathcal{S}_{tdj}$ used in constraints (9) which imposes the required platforms to engage debris d in order to relocate it to orbital slot j. In this formulation, S_{td} aims to impose a lower bound on the number of platforms required to engage debris d at time step t. This requirement can be beneficial in scenarios where large debris is targeted and a large $\Delta \boldsymbol{v}$ is required to generate a significant change in debris orbit.

The number of platforms to be used in the network is enforced by constraints (10), and the decision variables domain in the location formulation are defined as:

$$z_s \in \{0, 1\}, \qquad \forall s \in \mathcal{S} \tag{17a}$$

$$x_{td} \in \{0, 1\}, \quad \forall t \in \mathcal{T}, \forall d \in \mathcal{D} \tag{17b}$$

The MCLP formulation aims to maximize the realized network topology reward of the laser network during the mission time horizon $\mathcal{T}$, which is encoded in objective function (18):

$$\pi = \sum_{t \in \mathcal{T}} \sum_{d \in \mathcal{D}} R_{td} x_{td} \tag{18}$$

If an L2D engagement exists for debris d at time step t, then $x_{td} = 1$ and reward R_{td} associated is obtained. It is important to mention that if $R_{td} = 1, \forall t \in \mathcal{T}, \forall d \in \mathcal{D}$, the problem will yield the total number of potential engagements that the network has at the beginning of the L2D-ESP.

3.4.3. Mathematical Formulation

Piecing all constraints and the objective function together, the resulting MCLP optimization formulation that determines the location of the laser platforms to maximize the network topology reward is given as:

$$\begin{aligned} \max \quad & \text{Objective function (18)} \\ \text{s.t.} \quad & \text{Constraints (10), (16), (17a) and (17b)} \end{aligned}$$

The nature of the objective function and the lack of L2D engagement constraints similar to constraints (6b) incentivize the network to locate platforms at orbital slots that have a larger number of debris in range. Lastly, Table 2 presents the new parameters (params.) and decision variables (dec. vars.) introduced for the MCLP formulation.

3.5. Optimal Laser-to-Debris Engagement Scheduling Problem

In Sec. 3.4, we presented a framework to obtain the optimal location of the laser platforms to maximize the network topology rewards. In this section,

Table 2: Parameters and variables specific to the MCLP model.

Type	Symbol	Description
Params.	R_{td}	Network topology reward for debris d at time step t
	S_{td}	Engagement requirement for debris d at time step t ($S_{td} \in \mathbb{Z}_{\geq 1}$)
	W'_{tsd}	$\begin{cases} 1, & \text{if orbital slot } s \text{ can engage debris } d \text{ at time step } t \\ 0, & \text{otherwise} \end{cases}$
Dec. vars.	x_{td}	$\begin{cases} 1, & \text{if debris } d \text{ is engaged at time step } t \\ 0, & \text{otherwise} \end{cases}$

we build upon the assumption that the location of platforms is given and we maintain the engagement constraints from CLSP to derive the L2D-ESP.

Relaxing constraints (6a) and (10), the L2D-ESP is:

$$\begin{aligned} \max \quad & \text{Objective function (14)} \\ \text{s.t.} \quad & \text{Constraints (6b), (7), (8), (9), (12) and (13)} \end{aligned}$$

Even though constraints involving location decision variables z_s are relaxed, the scheduling problem continues to suffer from an exponential expansion of the solution space. To overcome this challenge, we propose a trade-off between the optimality of the solution and the computational runtime by implementing a myopic policy algorithm. The algorithm consists of breaking the problem into a set of coupled subproblems and solving them in a sequential manner such that the solution of a subproblem is used as initial conditions for the immediately subsequent subproblem. For the L2D-ESP, we parameterize the time step t and partition it into T coupled subproblems, where each subproblem solves the L2D-ESP for a time step t, therefore, each one of them has a solution space smaller than the original scheduling problem, making it lighter to solve.

3.5.1. Decision Variables

To solve the L2D-ESP by leveraging myopic policy, we parameterize time step t present in decision variables (12) and (13). Additionally, orbital slot index $i \in \mathcal{J}_{td}$ is relaxed from constraints (13) since the initial orbital slot for each subproblem is known. The new decision variables for the subproblem are defined as:

$$y_{pd}(t) = \begin{cases} 1, & \text{if platform } p \text{ engages debris } d \\ 0, & \text{otherwise} \end{cases} \tag{19a}$$

$$x_{dj}(t,i) = \begin{cases} 1, & \text{if debris } d \text{ relocates to orbital slot } j \\ 0, & \text{otherwise} \end{cases} \tag{19b}$$

3.5.2. Constraints and Objective Function

To define the engagement constraints, we parameterize time step t in constraints (6b) and (9). Furthermore, since no platform orbital slots are considered in the framework, we introduce the set of platforms $\mathcal{P}_{dj}(t) \subseteq \mathcal{P}$ with index p and cardinality $P_{dj}(t)$, that generate orbital slot $j \in \mathcal{J}_d(t)$ for debris $d \in \mathcal{D}$. Then, the engagement and linking constraints between variables for the subproblem are:

$$\sum_{d \in \mathcal{D}} y_{pd}(t) \leq 1, \qquad \forall p \in \mathcal{P} \tag{20a}$$

$$\sum_{p \in \mathcal{P}_{dj}(t)} y_{pd}(t) \geq P_{dj}(t) x_{dj}(t,i), \quad \forall d \in \mathcal{D}, \forall j \in \mathcal{J}_d(t) \tag{20b}$$

In addition to constraints (20b), we need to enforce each debris to relocate to at most one new orbital slot. To achieve this, we introduce constraints (21).

$$\sum_{j \in \mathcal{J}_d(t)} x_{dj}(t,i) \leq 1, \quad \forall d \in \mathcal{D} \tag{21}$$

The domains of the decision variables are given as:

$$x_{dj}(t,i) \in \{0,1\}, \quad \forall d \in \mathcal{D}, \forall j \in \mathcal{J}_d(t) \tag{22a}$$

$$y_{pd}(t) \in \{0,1\}, \qquad \forall p \in \mathcal{P}, \forall d \in \mathcal{D} \tag{22b}$$

To account for the debris remediation capacity of the network for each subproblem t, we derive the reward for every time step t from Eq. (5) by parameterizing indices t and i, given as:

$$R_{dj}(t,i) = C_d^0(t) + C_{dj}(t,i) + \alpha \Delta h_{dj}(t,i) + \beta M_d(t) \tag{23}$$

albeit we are solving subproblem t, we let $C_d^0(t) = C_{td}^0$ and $C_{dj}(t,i) = C_{tdij}$ with C_{td}^0 and C_{tdij} defined as in Eq. (5). Therefore, objective function (24) encodes the debris remediation capacity of the network for subproblem t.

$$V(t) = \sum_{d \in \mathcal{D}} \sum_{j \in \mathcal{J}_d(t)} R_{dj}(t,i) x_{dj}(t,i) \tag{24}$$

3.5.3. Mathematical Formulation

The optimization problem for a single subproblem t is formulated as:

$$\begin{aligned} \max \quad & \text{Objective function (24)} \\ \text{s.t.} \quad & \text{Constraints (20a), (20b) (21), (22a) and (22b)} \end{aligned}$$

Table 3 presents the sets, parameters, and decision variables specific to subproblem t.

As a result of implementing the myopic policy algorithm, we can obtain the network's debris remediation capacity over the entire mission horizon by summing up objective function (24) for all subproblems, as defined in Eq. (25).

$$V = \sum_{t \in \mathcal{T}} V(t) \tag{25}$$

Table 3: Specific sets, parameters, and variables for L2D-ESP subproblem t.

Type	Symbol	Description
Sets	$\mathcal{P}_{dj}(t)$	Set of laser platforms that generate orbital slot j for debris d (index p; cardinality $P_{dj}(t)$)
Params.	$R_{dj}(t,i)$	Debris remediation capacity reward
Dec. vars.	$y_{pd}(t)$	$\begin{cases} 1, & \text{if laser platform } p \text{ engages debris } d \\ 0, & \text{otherwise} \end{cases}$
	$x_{dj}(t,i)$	$\begin{cases} 1, & \text{if debris } d \text{ locates to orbital slot } j \\ 0, & \text{otherwise} \end{cases}$

4. Case Studies

To demonstrate the extension and flexibility of the proposed formulations against different mission environments, we present three case studies involving debris remediation missions for (1) small, (2) large, and (3) mixed debris populations (comprising both small and large debris) in the presence of 10 valuable assets. For each case study, we determine the optimal network topology of 10 laser platforms based on the given debris field using the MCLP, obtain its network topology reward, and then evaluate its debris remediation capacity using the L2D-ESP.

The results obtained for the optimal network of 10 space-based laser platforms are benchmarked against two baseline cases: (1) a single platform case and (2) a 10-platform case in an optimized Walker-Delta network. The first benchmark, against a single platform system, helps reveal the extent to which debris remediation capacity improves with additional platforms. The second benchmark is intended to compare the effectiveness of asymmetry in the network topology in the debris remediation capacity. Walker-Delta [32] is a symmetrical constellation pattern that enforces satellites to be placed in circular orbits, all of them having the same altitude and inclination, making them beneficial for missions that require global coverage. The Walker-Delta pattern is denoted as $P/O/F$, where P stands for the number of satellites (platforms), O for the number of orbital planes, and F for the phasing factor between satellites. To identify the optimized 10-platform Walker-Delta network, we performed an enumeration of every possible pattern given 10 platforms, resulting in 18 patterns. Additionally, we randomly selected 20 pairs of semi-major axes and inclinations from the set of platform's orbital slots and generated all possible combinations of Walker-Delta configurations using 10 satellites, resulting in 360 networks. Using a brute-force algorithm, we obtain from the pool of generated Walker-Delta networks the best-performing one (*i.e.,* the one that collects the highest network

topology reward) and obtain its debris remediation capacity leveraging the L2D-ESP. The orbital elements of the simulated debris remediation networks in the case studies along with a three-dimensional visualization of the platform's orbit and debris field are presented in Appendix B.

We adopt the laser and debris parameters from Ref. [24] (except for the perigee threshold). The laser system considered is a laser-diode-pumped solid-state oscillator-amplifier with an amplifier medium of Nd:YAG or ND:glass, which operates using 100 ps ultraviolet pulses at the 3rd harmonic of neodymium at a wavelength of 355 nm. We assume that the debris material composition is aluminum and that the laser platform varies the pulse energy to maintain the desired fluence and c_m values. Furthermore, we propagate the orbits of laser platforms and debris considering up to the J_2 perturbation. The epoch t_0 is set to February 26, 2024, at 04:30:51 Coordinated Universal Time. After an L2D engagement, we assume the debris periapsis radius remains constant, neglecting the influence of J_2 to reduce the computational runtime when computing C_{tdij}. Lastly, to avoid a computationally prohibitive optimization problem, we propose a trade-off between the number of time steps and debris considered, that is, a larger population will be simulated with fewer time steps and vice versa. Table 4 summarizes the parameters shared across all case studies.

Table 4: Common parameters to all case studies.

Parameter	Value	Unit
Primary mirror diameter	1.50	m
Momentum coupling coefficient, c_{m}	99	N/MW
Wavelength, λ	355	nm
Pulse length, τ	0.10	ns
Fluence on debris, φ	8.50	kJ/m^2
Beam quality factor	2	-
Perigee threshold, h^*	100	km
Number of platforms	10	-

4.1. Case Study 1: Small Debris Field

We consider a seven-day mission time horizon, uniformly discretized with a time step size of 130 s, adopted from Ref. [24]. The time step size is determined by the L2D engagement duration of 10 s, with a PRF of 56 Hz, plus an additional 120 s for the laser equipment's cooling. Table 5 presents the remaining laser and debris parameters.

The small debris field is initialized based on results from a simulation conducted using ESA's Meteoroid And Space debris Terrestrial Environment Reference (MASTER-8) model [5]. The simulation considers small debris over an altitude range of 186 km to 2000 km, which accounts for explosion/collision fragments, sodium-potassium droplets, solid rocket motor slag, and multi-layer insulation. The MASTER-8 outputs are provided as relative frequencies across

Table 5: Small debris remediation specific parameters.

Parameter	Value	Unit
Laser range	$[175, 325]$	km
Debris density	1	$\mathrm{kg/m^2}$
Time step size	130	s
Length L2D engagement	10	s
PRF	56	Hz
Pulse efficiency	0.50	-

100 altitude bins that discretized the low Earth orbit (LEO) altitude range of 100 km to 2000 km into bins having a width of 18.14 km. To initialize a representative small debris field across the LEO altitude band, 820 samples are drawn from the respective relative frequencies for each altitude bin. Figure 5a shows the small debris population per altitude bin. Each small debris object is assumed to be in a circular orbit with uniformly distributed values for the argument of periapsis, the argument of latitude, and right ascension of the ascending node (RAAN), bounded between 0 and 360 deg, and inclination ranging from 0 to 180 deg.

Next, we generate a set of orbital slots that laser platforms can take by defining an altitude range from 400 km to 1100 km, equally spaced in nine altitude layers. We adopt this range as it embraces the peak of operating satellites, outlined in Fig. 5b and the small debris population. Further, we define 10 steps for the argument of latitude and RAAN, uniformly spaced between 0 deg and 360 deg. In addition, we define 9 uniformly spaced steps for the inclination between 35 deg and 90 deg. All orbits are assumed to have an eccentricity of zero at the epoch.

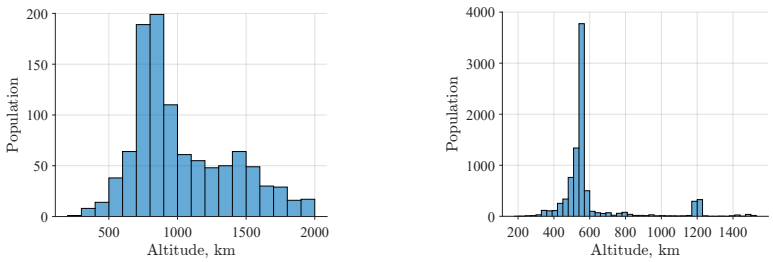

(a) Small debris population per altitude bin. (b) Active satellite population per altitude bin.

Figure 5: Active satellites and debris distribution per altitude bins.

For this specific case study, we are not considering valuable assets operating in the environment; consequently, $C_{td}^0 = C_{tdij} = 0$ for all $t \in \mathcal{T}, d \in \mathcal{D}, i \in \mathcal{J}_{td}, j \in \mathcal{J}_{t+1,d}$. Second, M_{td} is assumed to be equal for all $d \in \mathcal{D}$ due to the assumption that all debris has equal density.

4.1.1. Results and Discussions

The network topology reward obtained is $\pi^* = 9269$, and the retrieved optimal network topology consists of 10 platforms asymmetrically distributed. The optimal L2D-ESP is implemented with the optimal network topology obtained, retrieving a debris remediation capacity reward of $V^* = 3132.34$. Figure 6a provides a snapshot of the debris field with 10 laser platforms at time step $t = 11$, and Fig. 6b visualizes an L2D engagement over the Antarctic region at that same time step.

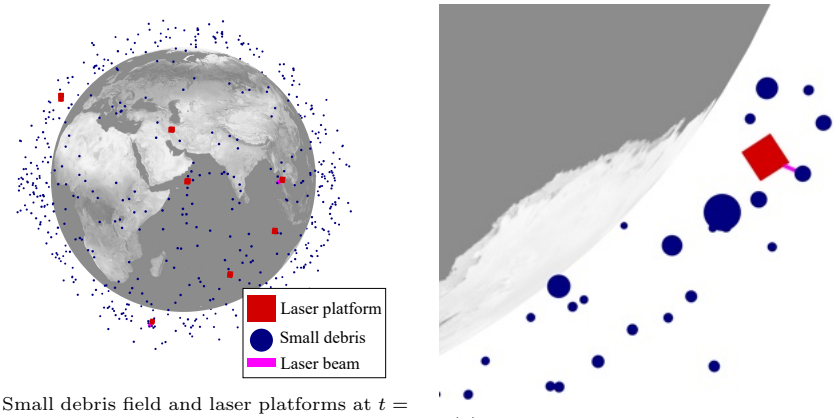

(a) Small debris field and laser platforms at $t = 11$.

(b) Detailed L2D engagement at $t = 11$.

Figure 6: 10-platform network for small debris remediation mission.

From the L2D optimization results it is possible to derive certain metrics that are useful for characterizing the mission performance, even though they are not the objective of the optimization. First, the network engages 599 small debris throughout the seven-day mission time horizon, representing the 73.04 % of the total population considered. Second, the number of debris deorbited during this time horizon is 422, or 51.46 % of the total population. Third, we understand debris nudging as the sum of the differences between the periapsis radius at the epoch and the end of the simulation for all engaged but not deorbited debris, yielding a value for the optimal 10-platform network of 64,707.56 km.

The single platform case collects a network topology reward of $\pi^* = 1038$ and has a debris remediation capacity of $V^* = 722.08$. The total number of engaged debris is 313 deorbiting a total of 29 and nudging debris 95,321.31 km. The adoption of 10 platforms over one increases by 88.80 % and 76.94 % the network topology reward π and the debris remediation capacity V, respectively. Considering the derived metrics, increasing the number of platforms leads to 93.12 % more debris deorbited. The single platform mission nudges debris 95,321.31 km outperforming the 10-laser platform by 43.31 %, given that the former is less successful in deorbiting objects, it has more debris objects contributing to this metric.

Lastly, we obtain a Walker-Delta network with pattern 10/1/0, an altitude

of 7303.14 km and inclination of 48.75 deg. The network topology reward obtained by the Walker-Delta network is $\pi = 7354$ and its debris remediation capacity is $V = 2927.24$. The derived metrics for this network exhibit that 538 debris are engaged, 382 are deorbited, and the network nudges debris a total of 63,801.59 km.

The debris remediation capacity of the network depends not only on the number of platforms but also on their distribution. Breaking the symmetry in the distribution of lasers leads to an increase of 20.66 % and 6.54 % in the network topology reward and the debris remediation capacity, respectively. Additionally, the MCLP-based network outperforms the symmetrical Walker-Delta network on the derived metrics as it deorbits 9.47 % more debris, and presents an increase of 1.40 % on the total debris periapsis radius difference with respect to the epoch.

4.2. Case Study 2: Large Debris Field

The mission time horizon is set to 31 days, uniformly discretized with a time step of 160 s. Each L2D engagement lasts 40 s, followed by a cooling period of 120 s. For the debris population, we adopt the 50 statistically most concerning debris objects as identified by Ref. [2]. For simplicity, we assume that all debris objects have the same cross-sectional area while retaining their actual masses as reported in Ref. [2]. With this approach, the magnitude of the delivered Δv is not constant among the considered debris field since it is inversely proportional to debris mass. To define the platform orbital slots, we maintain the values defined for Sec. 4.1 except for the altitude range, since the L2D range is larger we extend the altitude upper bound to 1400 km. We report the specific parameters used in this case study in Table 6.

Table 6: Large debris remediation specific parameters.

Parameter	Value	Unit
Laser range	$[300, 900]$	km
Time step size	160	s
Length L2D engagement	40	s
PRF	21	Hz
Pulse efficiency	1	-

4.2.1. Results and Discussions

The network topology reward obtained is $\pi^* = 20{,}330.23$ with an asymmetrical platform distribution, and its debris remediation capacity is $V^* = 26{,}826.56$. Figure 7a displays the large debris field and the 10 laser platforms at time step $t = 1314$ whereas Fig. 7b shows two L2D engagements. The first one consists of a single L2D engagement from one platform to debris; the second one is a collaborative L2D engagement from two platforms to one debris, highlighting

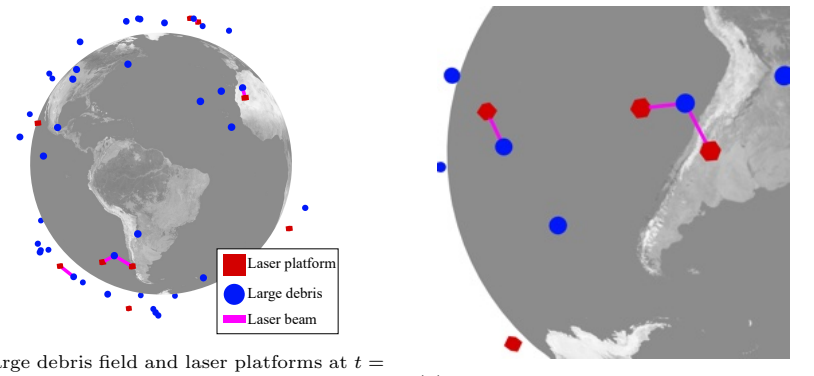

(a) Large debris field and laser platforms at $t = 1314$.

(b) Detailed L2D engagement at $t = 1314$.

Figure 7: 10-platform network for large debris only.

the significance of DVA and how the network leverages this concept to maximize rewards.

Similarly to the analysis carried out in Sec. 4.1.1, we derive metrics from the obtained results. The total number of L2D engagements during the operation of the mission is 20,225 and the debris that is engaged the most has a mass of 9000 kg. Considering that it is less likely to induce significant periapsis radius reductions due to L2D engagements at each individual time step given the large mass of debris, the term that accounts for debris mass in Eq. (23) weighs the most in the reward, which is reflected in the number of engagements that debris of higher mass receive. Further, the network nudges debris 941.54 km.

Changing the cardinality of the network and imposing only one platform into the MCLP problem formulation retrieves a network topology reward $\pi^* = 2916.35$ and a debris remediation capacity of $V^* = 6526.54$. The significant reduction in the number of platforms directly impacts the results by reducing 85.65 % and 75.67 % the network topology reward and the debris remediation capacity, respectively. The single platform performs 4163 L2D engagements, with the same most engaged debris object as the 10-platform network has. The difference with respect to the 10-platform network is 79.41 %. The single platform nudges debris 214.70 km signifying a decrement of 77.19 % compared to the 10-platform network.

The best-performing Walker-Delta network, with a pattern of 10/10/0, an altitude of 7040.64 km and an inclination of 76.25 km, achieves a network topology reward of $\pi = 11{,}255.10$ and a debris remediation capacity $V = 22{,}651.94$. The Walker-Delta network underperforms compared to the asymmetrical MCLP-based network by 44.63 % and 15.56 % for the network topology reward and debris remediation capacity, respectively. The total number of L2D engagements for the Walker-Delta network is 17,632, which is 12.82 % less than that of the optimal MCLP-based network, but it continues to have the most L2D engagements to a 9000 kg debris object. Lastly, the Walker-Delta network nudges

debris 975.45 km, compared to the 941.54 km obtained by leveraging the optimal network. This phenomenon can be associated with the fact that neither the MCLP formulation nor the L2D-ESP directly optimizes the difference in debris periapsis radius with respect to the epoch.

4.3. Case Study 3: Mixed Debris Field With Valuable Assets

In this case study, the mission horizon of seven days is uniformly discretized with a time step size of 160 s to encompass the L2D engagement and cooling times for small and large debris. Further, we maintain the laser operational ranges for small and large debris as defined in Sec. 4.1 and Sec. 4.2, respectively.

The small debris field is generated as in Sec. 4.1 and we define a population of 820 objects. The large debris field is the same from Sec. 4.2 in addition to defunct satellite COSMOS 2221 (NORAD ID: 22236) with an associated reward of $G_0 = 10^6$ during the network topology optimization, and $G_0 = 10^4$ for the L2D-ESP. Lastly, we define a set of 10 valuable assets $\mathcal{K} = \{k_1, \ldots, k_{10}\}$ and Table 7 presents their respective orbital elements defined at epoch t_0, with ω and ν as the argument of periapsis and true anomaly, respectively. The conjunction ellipsoid for all valuable assets is assumed to be a perfect sphere of radius 10 km.

Table 7: Orbital elements of valuable assets defined at epoch t_0.

Index	SMA, km	e	Incl., deg.	RAAN, deg	ω, deg.	ν, deg.
k_1	6862.80	0.0013	52.94	240.18	76.06	300.22
k_2	6933.20	0.0011	53.20	109.69	106.38	63.51
k_3	6921.01	0.0015	52.94	224.49	71.00	181.65
k_4	6924.25	0.0014	53.35	66.92	68.18	316.11
k_5	6874.50	0.0005	97.53	132.48	273.28	73.11
k_6	7131.61	0.0021	86.46	16.74	77.71	170.80
k_7	6917.09	0.0011	53.12	221.95	66.99	60.67
k_8	7565.34	0.0010	88.04	81.73	122.65	66.20
k_9	6955.44	0.0012	69.88	276.33	67.97	307.92
k_{10}	6796.97	0.0006	51.70	150.06	78.94	50.82

In addition to the 10 valuable assets, the mixed debris field study includes a known close conjunction event on February 28, 2024. The conjunction event was between the defunct satellite 22236 and the non-maneuverable operational NASA TIMED satellite (NORAD ID: 26998) with a reported miss distance of 20 m at the time of closest approach (TCA) [43]. In the simulated conjunction event within the mixed debris field, a miss distance of 2.30 km is observed at the TCA, corresponding to time step $t = 1081$.

4.3.1. Results and Discussions

The optimal 10-platform network achieves a network topology reward of $\pi^* = 7.10 \times 10^7$ and has a debris remediation capacity obtained of $V^* = 2.86 \times 10^5$. Figure 8a displays the mixed debris field and the 10 laser platforms at time

step $t = 7$. Figure 8b is a detailed view of the same scenario pinpointing into three L2D engagements. First, two platforms engage two large debris objects, second, a single platform engages small debris from a closer range.

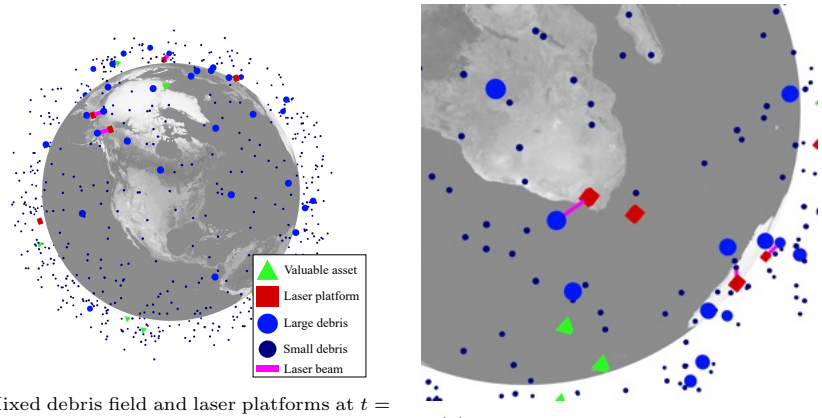

(a) Mixed debris field and laser platforms at $t = 7$.

(b) Detailed L2D engagement at $t = 7$.

Figure 8: 10-platform network for small and large debris.

The optimal 10-platform network engages 546 debris objects of various sizes, successfully deorbiting 141 small debris, and nudging debris 43,510.04 km. The conjunction event expected to occur at time step $t = 1081$ in this scenario is successfully avoided, with the miss distance between NASA satellite 26998 and defunct satellite 22236 increasing from 2.30 km to 2104.47 km after 17 L2D engagements during the imposed time step window $t \in [500, 622]$. The new minimum miss distance between the two objects is 545.91 km at time step $t = 103$ when the debris has not been engaged yet.

The baseline single platform case collects a network topology reward $\pi^* = 1.60 \times 10^7$ and has a debris remediation capacity of $V^* = 69{,}211.24$. Compared to the optimal 10-platform network, these values represent significant reductions of 77.46 % in network topology reward and 75.83 % in debris remediation capacity. The single platform engages with 228 debris, successfully deorbits 24 small debris, and nudges debris 25,733.06 km. These metrics present reductions of 82.97 % in the number of total debris deorbited and 40.85 % in the total distance nudged compared to the 10-platform network. The new closest approach between defunct satellite 22236 and satellite 26998 has a distance of 57.43 km at time step $t = 936$, and a new miss distance of 411.71 km at the original TCA corresponding to $t = 1081$.

The best-performing Walker-Delta network has a pattern 10/5/2 with an orbital altitude of 6953.14 km and an inclination of 76.25 deg. It achieves a network topology reward $\pi = 2.98 \times 10^5$ and a debris remediation capacity of $V = 1.23 \times 10^5$. When the same number of laser platforms is used but constrained to fit the symmetrical Walker-Delta pattern, there is a substantial reduction in both the network topology reward and debris remediation capacity

by 99.58 % and 56.90 %, respectively. The Walker-Delta network engages with 441 debris objects from which it successfully deorbits 129 of them, resulting in 8.51 % fewer than the optimal 10-platform network. The minimum miss distance between the active and defunct satellite is 545.94 km at time step $t = 103$, and even though the Walker-Delta does not engage the defunct satellite at the imposed time step window $t \in [500, 622]$, it does so before it, consequently, the relative distance between the two objects at time step $t = 1081$ is 2605.02 km.

4.4. General Discussions

Even though the case studies presented in this paper do not span all possible mission scenarios, we handpicked the most representative ones for debris remediation missions. Each mission scenario is uniquely characterized by a set of variables that condition the outcome of the space-based laser debris remediation mission. For the three different scenarios, we tested a triplet of networks, two of them optimally locate their one and 10 platforms exploiting the MCLP formulation considering the debris field distribution, and the remaining one is an optimized Walker-Delta network from a pool of 360.

Increasing the number of platforms from one to 10 leads to a significant rise in the debris remediation capacity of the network and its derived metrics. In all case studies, the debris remediation capacity improves close to 75 % when the number of platforms increases. The results obtained in all three case studies enable us to conclude that further increments in the debris remediation capacity and derived metrics can be achieved using the same number of platforms by breaking the symmetry of the network and determining the optimal location of platforms leveraging MCLP to deliver the additional increments. The MCLP provides flexibility in the location of laser platforms as it accounts for the mission environment defined and seeks to select the orbital slots, which are not constrained to follow a symmetrical pattern, that maximizes the network topology reward. The outcome of this formulation significantly improves the obtained debris remediation capacity, given by the L2D-ESP, as the platforms are better located relative to each other, the debris field considered, and, if any, the satellite-debris conjunction events.

5. Sensitivity Analysis

In this section, a sensitivity analysis is performed for different optimal networks, varying the number of platforms P from one to 10. Additionally, a 10-platform Walker-Delta network is included in the study. We define the cost of a network as the number of platforms used, and the benefit as the total rewards π^* and V^* obtained. All networks are simulated in the same mission environment adopted in Sec. 4.3.

Figure 9 highlights the rewards obtained by each network in the optimization problems, where 10-WD stands for the 10-platform Walker-Delta network. The leftmost bar plot of Fig. 9 presents the network topology reward π^*, demonstrating a positive correlation between the increment in the number of platforms

and the achieved reward. Further, all MCLP-based optimal networks obtain a higher reward with respect to the 10-platform Walker-Delta network. The center of Fig. 9 outlines the total debris remediation capacity reward V^* obtained leveraging the L2D-ESP. Concerning this metric, the Walker-Delta network is outperformed by MCLP-based networks with at least three platforms. Focusing on MCLP-based networks only, the obtained V^* does not maintain a monotonic increase with the increment in the number of platforms since adopting 8 platforms retrieves the highest reward. The rightmost bar plot of Fig. 9 breaks down the total debris remediation capacity reward by each term of Eq. (5); C_{tdij} term has been omitted since no networks perform L2D engagements that would trigger the penalty. First, C^0_{td}, the reward term that accounts for conjunctions if no L2D engagements occur, is obtained by all MCLP-based networks since the flexibility gained in the design space allows the network to engage defunct satellite 22236 in the specified time window, conversely, the Walker-Delta network is not able to collect any C^0_{td} reward. Moreover, the latter outperforms MCLP-based networks analyzing individual reward terms $\alpha\Delta h_{tdij}$, which accounts for the ratio between debris periapsis radius after the L2D engagement and periapsis radius threshold, and βM_{td}, the term that accounts for engaged debris mass, however, it is not conveyed in the total reward given its lack to obtain C^0_{td}, the term that weighs the most in Eq. (5).

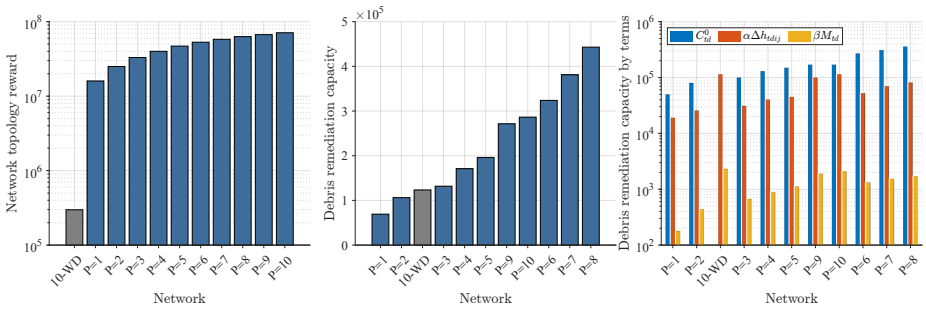

Figure 9: Obtained optimization rewards per network.

Figure 10 presents relevant mission metrics derived from the L2D-ESP, however, it is noteworthy to mention that objective function (24) is not designed to tackle any of them directly. The left bar plot of Fig. 10 presents the number of small debris deorbited per network, exhibiting a positive correlation between the number of deorbited objects and the number of platforms. The right bar plot of Fig. 10 reports the magnitude of nudged debris per network, where The Walker-Delta network is outperformed by all MCLP-based asymmetrical networks, and the 9-platform network provides the highest debris nudging value of 46,484.58 km.

In summary, this section outlines the performance of different mission architectures varying the number of space-based lasers used and their network topology. The results demonstrate the necessity of breaking the inherent symmetry of Walker-Delta networks. MCLP-based optimal networks with at least

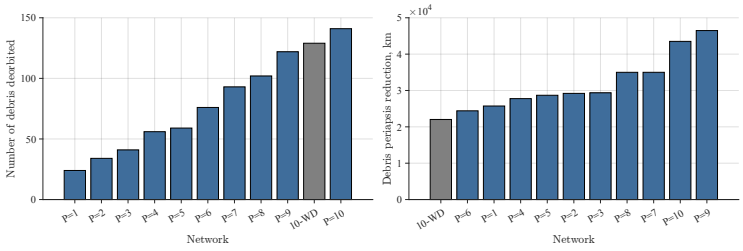

Figure 10: Optimization derived metrics per network.

three platforms outperform these symmetrical networks in terms of debris remediation capacity. Adopting MCLP expands the network topology design space, allowing for the retrieval of probably optimal network topologies that do not adhere to the symmetrical Walker-Delta pattern.

6. Limitations

From the results obtained throughout this paper, there are certain key points that need to be mentioned.

- First, this paper does not seek to endorse any specific laser platform system through the case studies presented. Instead, the case studies serve to demonstrate the extension and capabilities of the proposed optimization framework. Additionally, the optimization frameworks can be used as a testbed to determine the optimal location and operation for such a system, given a specific laser system.
- Second, increasing the number of platforms during the L2D-ESP does not guarantee a solution that is at least as good as one obtained with fewer platforms. This phenomenon is attributed to the use of a myopic policy algorithm, which cannot obtain certified globally optimal solutions. Furthermore, due to the sequential nature of the algorithm, all missions included in the sensitivity analysis share the same debris field at the initial epoch. However, after the first L2D engagement, the debris field is likely to differ across cases.
- Third, the proposed reward function aims to capture what we understand to be the most important figures of merit to consider in a debris remediation mission. Nevertheless, this does not ensure that the one presented in this paper is the best representation of these figures of merit for such missions.

7. Conclusions

This paper addresses the problem of remediating orbital debris of various sizes using a network of space-based lasers. We present an optimization

framework designed for both the configuration and operation of a network of cooperative space-based lasers, capable of deorbiting and nudging debris, as well as performing just-in-time collision avoidance based on any user-defined laser platform specifications.

Introducing the MCLP formulation to design debris remediation networks, for the first time, allows us to obtain its network topology while considering several variables of the mission environment, mainly the characteristics of the targeted debris field, the number and specifications of the laser platforms, and the operation of valuable assets in space. We propose the L2D-ESP which seeks to maximize the debris remediation capacity of the network during the operation of the mission. The latter leverages the novel concept of DVA, a collaborative engagement framework that enables achieving a higher degree of control over the L2D engagements.

We present two sets of experiments in this paper. The first one corresponds to the case studies where the main objective is to exhibit the applicability and extension of the optimization formulations proposed. Further, the different case studies enable us to conclude that the debris remediation capacity can be increased if (1) the number of platforms used in the network is incremented and (2) given the same number of laser platforms, breaking the symmetry of Walker-Delta networks by leveraging the MCLP formulation. The second set of experiments corresponds to the sensitivity analysis which ranges the number of platforms from one to 10 and includes a 10-platform Walker-Delta network. The results obtained outline that increasing the number of platforms can be beneficial up to a certain cardinality, after which either the debris remediation capacity or certain metrics of interest tend to decrease.

There are several avenues for future research. First, consider the stochasticity in L2D ablation processes, associated with pointing accuracy, beam incidence angle, and debris shape and material composition. Second, enhance the flexibility of the network by allowing platforms to reposition into different orbits, leveraging the concept of satellite constellation reconfiguration to maximize debris remediation capacity in a dynamic debris field. Lastly, explore various laser parameters, such as, but not limited to, input electrical power, PRF, pulse energy, and operational range, suitable for operation on small spacecraft. Consequently, a trade-off study, in the form of a cost-benefit analysis, can be conducted to determine the optimal location and operation of platforms by incorporating their size, mass, and laser parameters as decision variables.

Acknowledgment

This work was supported by an Early Career Faculty grant from NASA's Space Technology Research Grants Program under award No. 80NSSC23K1499. The authors would like to thank Gavin Baker for their valuable comments and suggestions, which helped improve the clarity and quality of this paper.

Appendix A. Location Optimization Formulation

In this section, we present a step-by-step justification for the adoption of MCLP to tackle the optimal design of the space-based laser network topology. The CLSP formulation introduced in Sec. 3.3 is given as:

$$\max \quad \sum_{t\in\mathcal{T}\setminus\{t_{T-1}\}} \sum_{d\in\mathcal{D}} \sum_{i\in\mathcal{J}_{td}} \sum_{j\in\mathcal{J}_{t+1,d}} R_{tdij}x_{tdij} \tag{14}$$

$$\text{s.t.} \quad W_{tsd}z_s \geq y_{tsd}, \qquad \forall t\in\mathcal{T}, \forall s\in\mathcal{S}, \forall d\in\mathcal{D} \tag{6a}$$

$$\sum_{d\in\mathcal{D}} y_{tsd} \leq 1, \qquad \forall t\in\mathcal{T}, \forall s\in\mathcal{S} \tag{6b}$$

$$\sum_{j\in\mathcal{J}_{t_1 d}} x_{t_0 d i_0 j} = 1, \qquad \forall d\in\mathcal{D} \tag{7}$$

$$\sum_{j\in\mathcal{J}_{t+1,d}} x_{tdij} - \sum_{v\in\mathcal{J}_{t-1,d}} x_{t-1,dvi} = 0, \quad \forall t\in\mathcal{T}\setminus\{t_0,t_{T-1}\}, \forall d\in\mathcal{D}, \forall i\in\mathcal{J}_{td} \tag{8}$$

$$\sum_{s\in\mathcal{S}_{tdj}} y_{tsd} \geq S_{tdj}x_{tdij}, \quad \forall t\in\mathcal{T}\setminus\{t_{T-1}\}, \quad \forall d\in\mathcal{D}, \forall i\in\mathcal{J}_{td}, \forall j\in\mathcal{J}_{t+1,d}\setminus\tilde{\mathcal{J}}_{t+1,d} \tag{9}$$

$$\sum_{s\in\mathcal{S}} z_s = P \tag{10}$$

$$z_s \in \{0,1\}, \qquad \forall s\in\mathcal{S} \tag{11}$$

$$y_{tsd} \in \{0,1\}, \qquad \forall t\in\mathcal{T}, \forall s\in\mathcal{S}, \forall d\in\mathcal{D} \tag{12}$$

$$x_{tdij} \in \{0,1\}, \quad \forall t\in\mathcal{T}\setminus\{t_{T-1}\}, \forall d\in\mathcal{D}, \forall i\in\mathcal{J}_{td}, \forall j\in\mathcal{J}_{t+1,d} \tag{13}$$

As described in Sec. 3.3, the tree structure in the problem's solution space makes it computationally prohibitive. To overcome this problem, we adopt a series of assumptions that impact decision variables, parameters, and sets to obtain a space-based platform location optimization formulation.

The core assumption to overcome the tree structure is that debris maintains its initial orbit defined at t_0 during the entire mission. The consequences of this statement are several; first, debris cannot be deorbited, which makes the debris field constant over time. Second, debris orbital slot indices i, j can be dropped, consequently constraints (7) and (8) are relaxed. Third, given that orbital slot indices are dropped, CLSP decision variables x_{tdij} are now defined as:

$$x_{td} = \begin{cases} 1, & \text{if debris } d \text{ is engaged at time step } t \\ 0, & \text{otherwise} \end{cases}$$

As a result of dropping relocation indices, reward R_{tdij} defined in Eq. (5) is recasted as $R_{td} = C^0_{td} + M_{td}$. Removing Δh_{tdij} forbids the optimization model

to be informed about the post-L2D engagement behavior of debris (*i.e.* whether debris periapsis radius increases or decreases). To overcome this situation, we redefine W_{tsd} as W'_{tsd} where the latter incorporates as an additional requirement that debris periapsis radius after an L2D engagement has to be lower than its initial one.

With the described assumptions and relaxations, the derived formulation is:

$$\max \quad \sum_{t\in\mathcal{T}}\sum_{d\in\mathcal{D}} R_{td}x_{td} \tag{18}$$

$$\text{s.t.} \quad W'_{tsd}z_s \geq y_{tsd}, \qquad \forall t\in\mathcal{T}, \forall s\in\mathcal{S}, \forall d\in\mathcal{D} \tag{A.2a}$$

$$\sum_{d\in\mathcal{D}} y_{tsd} \leq 1, \qquad \forall t\in\mathcal{T}, \forall s\in\mathcal{S} \tag{6b}$$

$$\sum_{s\in\mathcal{S}_{td}} y_{tsd} \geq S_{td}x_{td}, \qquad \forall t\in\mathcal{T}, \forall d\in\mathcal{D} \tag{A.2b}$$

$$\sum_{s\in\mathcal{S}} z_s = P, \tag{10}$$

$$z_s \in \{0,1\}, \qquad \forall s\in\mathcal{S} \tag{11}$$

$$y_{tsd} \in \{0,1\}, \qquad \forall t\in\mathcal{T}, \forall s\in\mathcal{S}, \forall d\in\mathcal{D} \tag{12}$$

$$x_{td} \in \{0,1\}, \qquad \forall t\in\mathcal{T}, \forall d\in\mathcal{D} \tag{17b}$$

Even though relocation constraints are relaxed, the structure of the problem inherits the location-scheduling structure of the CLSP, since y_{tsd} are the L2D engagement scheduling decision variables that dictate whether an L2D engagement occurs from a platform located at slot s to debris d at time step t. Consequently, despite the fact that the new formulation does not have a tree structure, the dimension of decision variables $y_{tsd} \in \{0,1\}^{T\times S\times D}$ can make the problem computationally prohibitive. On top of that, given that the reward does not account for debris orbit changes, the formulation will tend to assign to each platform those orbital slots that maximize engagement with debris of larger mass. Given two debris d_1 and d_2 with masses $m_{d_1} < m_{d_2}$ and $C^0_{td_1} = C^0_{td_2} = 0$, then $M_{td_1} < M_{td_2}$ and consequently $R_{td_1} < R_{td_1}$. However, throughout the L2D-ESP where changes in debris periapsis are considered, if $\Delta h_{td_1ij} \gg \Delta h_{td_2ij}$, then:

$$\alpha\Delta h_{td_1ij} + \beta M_{td_1} > \alpha\Delta h_{td_1ij} + \beta M_{td_1}$$
$$R_{td_1ij} > R_{td_2ij}$$

outlining that the outcome, which corresponds to the optimal network that maximizes reward R_{td}, can overlook platform orbital slots that collect higher debris remediation rewards during the L2D-ESP.

To tackle this problem, and considering that it is not proper to perform L2D assignments if debris change in orbit is neglected, we propose to relax CLSP L2D engagement scheduling decision variables y_{tsd}. Consequently, constraints (6a), (6b), (9) and (12) are dropped. The resulting optimization problem

is given as:

$$\max \quad \sum_{t\in\mathcal{T}}\sum_{d\in\mathcal{D}} R_{td}x_{td} \tag{18}$$

$$\text{s.t.} \quad \sum_{s\in\mathcal{S}} z_s = P, \tag{10}$$

$$z_s \in \{0,1\}, \qquad \forall s \in \mathcal{S} \tag{11}$$

$$x_{td} \in \{0,1\}, \qquad \forall t \in \mathcal{T}, \forall d \in \mathcal{D} \tag{17b}$$

However, the new problem lacks coupling constraints that link location decision variables z_s and decision variables x_{td} such that L2D engagements with debris d occur only if a platform is occupying an orbital slot such that $W_{tsd} = 1$. Inspired by constraints (A.2a) and (A.2b), we introduce the new coupling constraints given as:

$$\sum_{s\in\mathcal{S}} W'_{tsd} z_s \geq S_{td} x_{td}, \quad \forall t \in \mathcal{T}, \forall d \in \mathcal{D} \tag{16}$$

where x_{td} are activated if at least S_{td} platforms perform L2D ablation on debris d at time step t. Hence, the formulation imposes a minimum number of platforms required to obtain debris' reward R_{td} at time step t. Consequently, the optimal laser network topology design problem is given as:

$$\max \quad \sum_{t\in\mathcal{T}}\sum_{d\in\mathcal{D}} R_{td}x_{td} \tag{18}$$

$$\text{s.t.} \quad \sum_{s\in\mathcal{S}} z_s = P \tag{10}$$

$$\sum_{s\in\mathcal{S}} W'_{tsd} z_s \geq S_{td} x_{td}, \quad \forall t \in \mathcal{T}, \forall d \in \mathcal{D} \tag{16}$$

$$z_s \in \{0,1\}, \qquad \forall s \in \mathcal{S} \tag{17a}$$

$$x_{td} \in \{0,1\}, \qquad \forall t \in \mathcal{T}, \forall d \in \mathcal{D} \tag{17b}$$

where its structure resembles the well-known MCLP [29].

Appendix B. 3D Illustrations and Case Studies Result's Orbital Elements

We report the corresponding orbital elements of the results obtained in Sec. 4 along with the 3D visualization of the debris remediation network with the platform's orbits in the ECI reference frame. Figures B.11, B.12 and B.13 display for $P = 1, 10$ and the Walker-Delta network the debris remediation networks for the small, large and mixed debris field cases, respectively. Tables B.8, B.9 and B.10 present the orbital elements for the $P = 1, 10$ and Walker-Delta networks for the small, large, and mixed debris field cases, respectively.

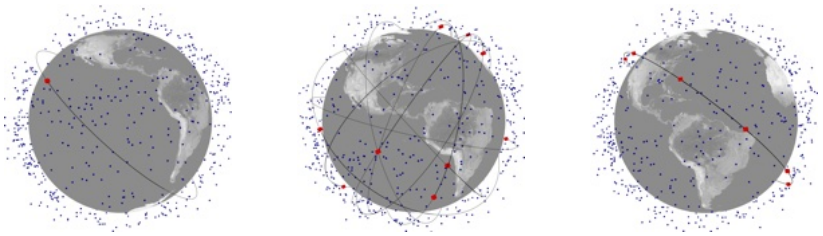

(a) $P = 1$. (b) $P = 10$. (c) $P = 10$ Walker-Delta.

Figure B.11: Small debris field case study: 3D visualization of debris remediation networks with orbits in ECI at $t = t_0$.

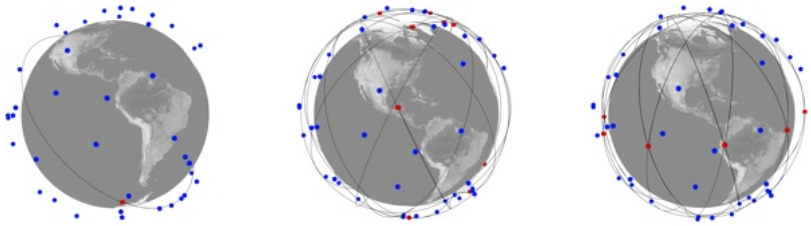

(a) $P = 1$. (b) $P = 10$. (c) $P = 10$ Walker-Delta.

Figure B.12: Large debris field case study: 3D visualization of debris remediation networks with orbits in ECI at $t = t_0$.

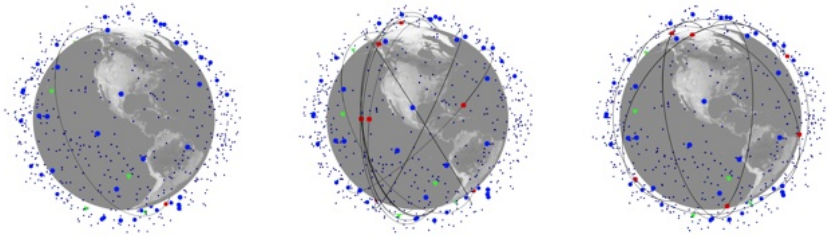

(a) $P = 1$. (b) $P = 10$. (c) $P = 10$ Walker-Delta.

Figure B.13: Mixed debris field case study: 3D visualization of debris remediation networks with orbits in ECI at $t = t_0$.

Table B.8: Orbital elements of platforms, defined at epoch t_0, for the small debris field case study.

Network	Sat. index	SMA, km	Incl., deg.	RAAN, deg	Arg. of Latitude, deg.
Single platform	p_1	7390.64	62.50	280	160
10 platform	p_1	7040.64	48.75	120	80
	p_2	7040.64	69.37	320	200
	p_3	7128.14	35	80	320
	p_4	7128.14	35	120	360
	p_5	7128.14	83.12	120	120
	p_6	7215.64	55.62	160	320
	p_7	7303.14	35	160	40
	p_8	7303.14	35	160	80
	p_9	7303.14	35	320	280
	p_{10}	7390.64	62.50	280	160
10 platform Walker-Delta	p_1	7303.14	48.75	0	0
	p_2	7303.14	48.75	0	36
	p_3	7303.14	48.75	0	72
	p_4	7303.14	48.75	0	108
	p_5	7303.14	48.75	0	144
	p_6	7303.14	48.75	0	180
	p_7	7303.14	48.75	0	216
	p_8	7303.14	48.75	0	252
	p_{10}	7303.14	48.75	0	324

Table B.9: Orbital elements of platforms, defined at epoch t_0, for the large debris field case study.

Network	Sat. index	SMA, km	Incl., deg.	RAAN, deg	Arg. of Latitude, deg.
Single platform	p_1	7215.64	69.375	280	240
10 platform	p_1	7128.14	90	40	80
	p_2	7215.64	62.50	80	80
	p_3	7215.64	62.50	120	80
	p_4	7215.64	62.50	160	120
	p_5	7215.64	69.375	200	80
	p_6	7215.64	69.375	280	240
	p_7	7215.64	69.375	320	160
	p_8	7215.64	69.375	0	240
	p_9	7215.64	76.25	40	120
	p_{10}	7215.64	83.125	240	320
10 platform Walker-Delta	p_1	7040.64	76.25	0	0
	p_2	7040.64	76.25	36	0
	p_3	7040.64	76.25	72	0
	p_4	7040.64	76.25	108	0
	p_5	7040.64	76.25	144	0
	p_6	7040.64	76.25	180	0
	p_7	7040.64	76.25	216	0
	p_8	7040.64	76.25	252	0
	p_9	7040.64	76.25	288	0
	p_{10}	7040.64	76.25	324	0

Table B.10: Orbital elements of platforms, defined at epoch t_0, for the mixed debris field case study.

Network	Sat. index	SMA, km	Incl., deg.	RAAN, deg	Arg. of Latitude, deg.
Single platform	p_1	6953.14	55.625	280	280
10 platform	p_1	6778.14	76.25	280	40
	p_2	6778.14	76.25	280	80
	p_3	6865.64	62.50	120	280
	p_4	6865.64	76.25	280	160
	p_5	6865.64	90	280	160
	p_6	6953.14	41.875	120	40
	p_7	6953.14	55.625	280	280
	p_8	7040.64	62.50	320	0
	p_9	7128.14	83.125	280	120
	p_{10}	7390.64	83.125	280	40
10 platform Walker-Delta	p_1	6953.14	76.25	0	0
	p_2	6953.14	76.25	0	180
	p_3	6953.14	76.25	72	72
	p_4	6953.14	76.25	72	252
	p_5	6953.14	76.25	144	144
	p_6	6953.14	76.25	144	324
	p_7	6953.14	76.25	216	216
	p_8	6953.14	76.25	216	36
	p_9	6953.14	76.25	288	288
	p_{10}	6953.14	76.25	288	108

References

[1] Tim Fernholz, Payload, A satellite conjunction scare marks an "inflection point" in collision risk, https://payloadspace.com/a-satellite-conjunction-scare-marks-an-inflection-point-in-collision-risk (2024).

[2] D. McKnight, R. Witner, F. Letizia, S. Lemmens, L. Anselmo, C. Pardini, A. Rossi, C. Kunstadter, S. Kawamoto, V. Aslanov, J.-C. Dolado Perez, V. Ruch, H. Lewis, M. Nicolls, L. Jing, S. Dan, W. Dongfang, A. Baranov, D. Grishko, Identifying the 50 statistically-most-concerning derelict objects in leo, Acta Astronautica 181 (2021) 282–291. doi:10.1016/j.actaastro.2021.01.021.

[3] T. J. Colvin, J. Karcz, G. Wusk, Cost and benefit analysis of orbital debris remediation (2023).
URL https://ntrs.nasa.gov/citations/20230002817

[4] Orbital Debris Interagency Working Group Subcommittee on Space Weather, Security and Hazards. National Science and Technology Council, National orbital debris research and development plan (2021).
URL https://trumpwhitehouse.archives.gov/wp-content/uploads/2021/01/National-Orbital-Debris-RD-Plan-2021.pdf

[5] European Space Agency, Maintenance of the esa master model, https://sdup.esoc.esa.int/master/downloads/documentation/7.02/MASTER_Final_Report.pdf (June 2011).

[6] S. Mark Smith, Anti-satellite weapons: History, types and purpose, https://www.space.com/anti-satellite-weapons-asats (2022).

[7] European Space Agency, About space debris, https://www.esa.int/Space_Safety/Space_Debris/About_space_debris (2016).

[8] S. Tereza Pultarova, Old soviet satellite breaks apart in orbit after space debris collision, https://www.space.com/soviet-satellite-breaks-apart-after-debris-strike (2023).

[9] D. J. Kessler, B. G. Cour-Palais, Collision frequency of artificial satellites: The creation of a debris belt, Journal of Geophysical Research: Space Physics 83 (A6) (1978) 2637–2646. doi:10.1029/JA083iA06p02637.

[10] N. L. Johnson, E. G. Stansbery, The new nasa orbital debris mitigation procedural requirements and standards, Acta Astronautica 66 (3) (2010) 362–367. doi:10.1016/j.actaastro.2009.07.009.

[11] I. Sharf, B. Thomsen, E. M. Botta, A. K. Misra, Experiments and simulation of a net closing mechanism for tether-net capture of space debris, Acta Astronautica 139 (2017) 332–343. doi:10.1016/j.actaastro.2017.07.026.

[12] D. McKnight, F. Di Pentino, A. Kaczmarek, S. Knowles, Detumbling Rocket Bodies in Preparation for Active Debris Removal, in: L. Ouwehand (Ed.), 6th European Conference on Space Debris, Vol. 723 of ESA Special Publication, 2013, p. 91.

[13] M. Shan, J. Guo, E. Gill, Review and comparison of active space debris capturing and removal methods, Progress in Aerospace Sciences 80 (2016) 18–32. doi:10.1016/j.paerosci.2015.11.001.

[14] W. Pulliam, et al., Catcher's mitt final report, Defense Advanced Research Projects Agency Rept. Ad1016641, Arlington, VA (2011).

[15] N. Takeichi, N. Tachibana, A tethered plate satellite as a sweeper of small space debris, Acta Astronautica 189 (2021) 429–436. doi:10.1016/j.actaastro.2021.08.051.

[16] M. A. Foster, Practical system to remove lethal untracked orbital debris, Journal of Aerospace Information Systems 19 (10) (2022) 661–667. doi:10.2514/1.I010985.

[17] J. Mason, J. Stupl, W. Marshall, C. Levit, Orbital debris–debris collision avoidance, Advances in Space Research 48 (10) (2011) 1643–1655. doi:10.1016/j.asr.2011.08.005.

[18] S. Scharring, J. Kästel, G. Wagner, W. Riede, E. M. Klein, C. Bamann, E. Döberl, D. Weinzinger, W. Promper, T. Flohrer, A. Di Mira, Potential of using ground-based high-power lasers to decelerate the evolution of space debris in leo, in: 8th European Conference on Space Debris, 2021.
URL https://elib.dlr.de/142421/

[19] C. R. Phipps, A laser-optical system to re-enter or lower low earth orbit space debris, Acta Astronautica 93 (2014) 418–429. doi:10.1016/j.actaastro.2013.07.031.

[20] B. Esmiller, C. Jacquelard, H.-A. Eckel, E. Wnuk, Space debris removal by ground-based lasers: main conclusions of the european project cleanspace, Appl. Opt. 53 (31) (2014) I45–I54. doi:10.1364/AO.53.000I45.

[21] W. O. Schall, Laser radiation for cleaning space debris from lower earth orbits, Journal of Spacecraft and Rockets 39 (1) (2002) 81–91. doi:10.2514/2.3785.

[22] C. R. Phipps, C. Bonnal, A spaceborne, pulsed uv laser system for re-entering or nudging leo debris, and re-orbiting geo debris, Acta Astronautica 118 (2016) 224–236. doi:10.1016/j.actaastro.2015.10.005.

[23] R. Soulard, M. N. Quinn, T. Tajima, G. Mourou, Ican: A novel laser architecture for space debris removal, Acta Astronautica 105 (1) (2014) 192–200. doi:10.1016/j.actaastro.2014.09.004.

[24] C. R. Phipps, L' adroit–a spaceborne ultraviolet laser system for space debris clearing, Acta Astronautica 104 (1) (2014) 243–255. doi:10.1016/j.actaastro.2014.08.007.

[25] S. Bondarenko, S. Lyagushin, G. Shifrin, Prospects of using lasers and military space technology for space debris removal, in: Second European Conference on Space Debris, Organised by ESA, held 17-19 March, 1997, ESOC, Darmstadt, Germany (1997), ESA-SP 393., p. 703, Vol. 393, 1997, p. 703.

[26] Y. Fang, J. Pan, Y. Luo, C. Li, Effects of deorbit evolution on space-based pulse laser irradiating centimeter-scale space debris in leo, Acta Astronautica 165 (2019) 184–190. doi:10.1016/j.actaastro.2019.09.010.

[27] C. Bonnal, D. McKnight, C. Phipps, C. Dupont, S. Missonnier, L. Lequette, M. Merle, S. Rommelaere, Just in time collision avoidance – a review, Acta Astronautica 170 (2020) 637–651. doi:10.1016/j.actaastro.2020.02.016.

[28] S. Scharring, J. Wilken, H.-A. Eckel, Laser-based removal of irregularly shaped space debris, Optical engineering 56 (1) (2017) 011007–011007. doi:10.1117/1.OE.56.1.011007.

[29] R. Church, C. R. Velle, The maximal covering location problem, Papers in Regional Science 32 (1) (1974) 101–118. doi:10.1111/j.1435-5597.1974.tb00902.x.

[30] H. Lee, K. Ho, Regional constellation reconfiguration problem: Integer linear programming formulation and lagrangian heuristic method, Journal of Spacecraft and Rockets 60 (6) (2023) 1828–1845. doi:10.2514/1.A35685.

[31] D. O. Williams Rogers, S.-W. Kim, M. Lee, Y.-H. Kim, H. Lee, Designing optimal satellite constellation patterns with facility location problem models and mixed integer linear programming, in: ASCEND 2023, 2023, p. 4658. doi:10.2514/6.2023-4658.

[32] J. G. Walker, Satellite constellations, Journal of the British Interplanetary Society 37 (1984) 559.

[33] P. Lorazo, L. J. Lewis, M. Meunier, Short-pulse laser ablation of solids: From phase explosion to fragmentation, Phys. Rev. Lett. 91 (2003) 225502. doi:10.1103/PhysRevLett.91.225502.

[34] S. Amoruso, Modeling of uv pulsed-laser ablation of metallic targets, Applied Physics A 69 (1999) 323–332. doi:10.1007/s003390051008.

[35] M. Stafe, A. Marcu, N. N. Puscas, Pulsed Laser Ablation of Solids, Springer, 2014.

[36] P. Battocchio, J. Terragni, N. Bazzanella, C. Cestari, M. Orlandi, W. J. Burger, R. Battiston, A. Miotello, Ballistic measurements of laser ablation generated impulse, Measurement Science and Technology 32 (1) (2020) 015901. doi:10.1088/1361-6501/abace6.

[37] T. J. Settecerri, J. E. Beraun, Laser debris sweeper for the space station freedom, in: Proceedings of the First European Conference on Space Debris, Darmstadt, Germany, 1993, pp. 471–477.

[38] J. Wilken, Modelling of laser-based thrust generation for space debris removal, Ph.D. thesis, Technische Universität Braunschweig (2015).
URL https://elib.dlr.de/95780/

[39] D. A. Liedahl, S. B. Libby, A. Rubenchik, Momentum transfer by laser ablation of irregularly shaped space debris, in: AIP Conference Proceedings, Vol. 1278, American Institute of Physics, 2010, pp. 772–779. doi:10.1063/1.3507171.

[40] D. Liedahl, A. Rubenchik, S. B. Libby, S. Nikolaev, C. R. Phipps, Pulsed laser interactions with space debris: target shape effects, Advances in Space Research 52 (5) (2013) 895–915. doi:10.1016/j.asr.2013.05.019.

[41] S. Scharring, R.-A. Lorbeer, H.-A. Eckel, Numerical simulations on laser-ablative micropropulsion with short and ultrashort laser pulses, Transactions Of The Japan Society For Aeronautical And Space Sciences, Aerospace Technology Japan 14 (ists30) (2016) Pb_69–Pb_75. doi:10.2322/tastj.14.Pb_69.

[42] J.-C. Liou, An active debris removal parametric study for leo environment remediation, Advances in Space Research 47 (11) (2011) 1865–1876. doi:10.1016/j.asr.2011.02.003.

[43] Space.com, Near miss! nasa satellite, dead russian spacecraft zoom past each other in orbit, https://www.space.com/near-collision-nasa-timed-satellite-russian-space-junk (2024).